Advances in sperm analysis: techniques, discoveries and applications

Changsheng Dai[1], *Zhuoran Zhang*[1], *Guanqiao Shan*[1], *Lap-Tak Chu*[1], *Zongjie Huang*[1], *Sergey Moskovstev*[2], *Clifford Librach*[2], *Keith Jarvi*[3,4]✉ *and Yu Sun*[1,5,6,7]✉

Abstract | Infertility affects one in six couples worldwide, and fertility continues to deteriorate globally, partly owing to a decline in semen quality. Sperm analysis has a central role in diagnosing and treating male factor infertility. Many emerging techniques, such as digital holography, super-resolution microscopy and next-generation sequencing, have been developed that enable improved analysis of sperm motility, morphology and genetics to help overcome limitations in accuracy and consistency, and improve sperm selection for infertility treatment. These techniques have also improved our understanding of fundamental sperm physiology by enabling discoveries in sperm behaviour and molecular structures. Further progress in sperm analysis and integrating these techniques into laboratories and clinics requires multidisciplinary collaboration, which will increase discovery and improve clinical outcomes.

Infertility affects 113 million people worldwide[1], and one in six couples need the help of assisted reproduction techniques (ARTs) to have a child[2]. Fertility rate, defined as the number of live births per couple, declined globally by 53% between 1960 and 2017 (REFS[3,4]). Male factor infertility is present in ~40% of infertile couples[2]. Mounting evidence suggests that fertility in men is declining, and sperm counts decreased by ~50% over the past 50 years globally[5,6]. Data from multiple centres have supported this observation of a temporal decline in sperm counts: one study from Scotland reported a considerable decrease in sperm concentration from 75.0×10^6/ml to 55.9×10^6/ml between 1994 and 2005 (REF.[7]), and a study from the USA found that sperm concentration among potential sperm donors decreased from 112×10^6/ml to 78×10^6/ml between 2003 and 2013 (REF.[8]). These changes are hypothesized to be caused by lifestyle and environmental changes, such as smoking and exposure to pollution[3,9].

Sperm analysis has a central role in the diagnosis and treatment of male factor infertility. According to the WHO[10], classic sperm analysis includes the measurement of semen volume, sperm concentration, the percentage of motile sperm and the fraction of sperm with normal morphology. Differences in sperm concentration, motility and morphology are used to diagnose men as fertile or subfertile[11]. Normal sperm motility and morphology have been positively correlated with fertilization and pregnancy rates[12–14]. Other clinical tests for sperm analysis in common use are based on genetic analysis, including the measurement of DNA damage and chromosome aberration[15,16]. Sperm DNA damage is caused by a variety of factors, including advanced paternal age (>40 years), oxidative stress, abortive apoptosis, aberrant protamine expression, defects in chromatin maturation and infection[17]. Sperm chromosome aberrations are caused by abnormal cell division[18]. DNA damage and chromosome aberrations lead to increased rates of pregnancy loss, and high rates of sperm DNA damage have been reported to reduce live birth rates following in vitro fertilization (IVF) by ~50%[19,20].

A variety of treatments are available for men with subfertility, among which ARTs including intrauterine insemination (IUI), IVF and intracytoplasmic sperm injection (ICSI)[21] are most commonly used. In IUI, a portion of semen, processed using techniques such as density gradient centrifugation, is inseminated into the uterus through a catheter and in IVF, processed sperm are incubated with oocytes in a Petri dish[22]. ICSI is performed by injecting a single sperm chosen by an embryologist into an oocyte with a sharp micropipette[22]. Since the birth of the first child conceived using ART in 1978, more than 8 million children have been born using ART treatment[23]. In North America ~200,000 ART cycles are performed yearly[24], and in Europe >900,000 cycles were performed in 2016 (REF.[25]). However, infertility treatment using ART raises concerns about bypassing the natural selection of sperm in the female reproductive tract, and that suboptimal sperm could be selected for use in IVF or ICSI[26]. The traditional technologies used for sperm sorting, such as density gradient centrifugation and swim-up assay, cannot select sperm with optimal DNA quality[22]. Using sperm with high DNA fragmentation for infertility treatment can cause embryo

[1]*Department of Mechanical and Industrial Engineering, University of Toronto, Toronto, Canada.*

[2]*CReATe Fertility Centre, Toronto, Canada.*

[3]*Division of Urology, Mount Sinai Hospital, Toronto, Canada.*

[4]*Department of Surgery, University of Toronto, Toronto, Canada.*

[5]*Institute of Biomaterials & Biomedical Engineering, University of Toronto, Toronto, Canada.*

[6]*Department of Electrical and Computer Engineering, University of Toronto, Toronto, Canada.*

[7]*Department of Computer Science, University of Toronto, Toronto, Canada.*

✉*e-mail: Keith.Jarvi@sinaihealth.ca; yu.sun@utoronto.ca*

https://doi.org/10.1038/s41585-021-00472-2

Key points

- Technical advances have improved the accuracy, speed and efficiency in the analysis of sperm motility, morphology and genetics.
- Advances in sperm analysis improve sperm selection for infertility treatment by measuring sperm behaviour and biomarkers of fertility potential.
- Discoveries in sperm locomotion and behaviour improve understanding of sperm motion and guidance within the female reproductive tract.
- Analyses of sperm structure and molecules such as CatSper channels and ubiquitin increase understanding of sperm physiology and contribute to the identification of biomarkers of fertility potential.
- Further progress in sperm analysis promises non-invasive testing for sperm selection, increased efficiency and accuracy via automation and artificial intelligence, and improved access to point-of-care assays.

arrest and pregnancy loss[27]; thus, techniques such as microfluidics[28] and hyaluronic acid binding[29] have been used to mimic the geometry and microenvironment of the female reproductive tract, and apoptotic markers[30] have been used to differentiate sperm. Although the sperm selected using these techniques demonstrated lower DNA fragmentation than observed using traditional techniques, the value of these techniques for improving ART success rates has not been validated[30,31]. The sperm that are capable of successfully navigating the female reproductive tract are the result of millions of years of evolution[32]; thus, identifying the attributes of these sperm can enable improved sperm analysis and optimal sperm selection for ART.

Technologies for sperm analysis have remained relatively unchanged, but a number of novel methods have now been developed that aid evaluation of sperm motility, morphology and genetics to improve diagnosis and treatment of male factor infertility. New techniques such as computer vision-based sperm tracking[33] and digital holography[34] have been developed to quantitatively measure sperm motility. Traditional morphology measurement relies on fixation and staining of sperm[10], rendering the analysed sperm unusable for infertility treatment. Non-invasive, high-magnification imaging[35] has been developed and can aid in selecting sperm with normal morphology. For sperm DNA damage measurement, traditional methods, such as the sperm chromatin structure assay (SCSA)[15], make the measured sperm unusable for treatment. To overcome this limitation, non-invasive approaches, such as Raman spectroscopy[36,37], have been studied. Next-generation sequencing (NGS) provides more accurate and comprehensive measurement than the commonly used fluorescence in situ hybridization (FISH) test for chromosomal analysis[38,39]. Sperm isolation techniques also have an important role in infertility treatment. For example, microfluidic devices have been developed that mimic the environment of the female reproductive tract to select sperm with high fertilization potential[40–42]. Hyaluronic acid, which surrounds an oocyte, has been used to physiologically select sperm, and annexin V can effectively identify apoptotic sperm and is used in magnetically activated cell sorting for sperm selection[43].

Advances in sperm analysis also have enabled new discoveries about sperm behaviour and structure. Sperm were found to swim along helices and chiral ribbons[44,45] within a 3D space, and swim in slithering mode within a confined space[46]. They also exhibit distinct behaviours such as boundary following[47] and corner turning[28] in microchannels, which improves our understanding of sperm locomotion within the female reproductive tract. To overcome the diffraction limit of light microscopy, super-resolution microscopy has been used to reveal sperm ultrastructures, such as proteins involved in motion regulation[48] and the acrosome reaction[49]. Using immunostaining and mass spectrometry, biomarkers have been identified such as ubiquitin[50], TEX101 (REF.[51]) and HspA2 (REF.[52]) that indicate sperm abnormality, obstructive azoospermia and sperm maturation, respectively.

Newly developed techniques improve spatial and temporal resolution for sperm analysis. They have the potential to predict fertility outcomes and enable standardized selection of optimal sperm for use in ART. These techniques also enable discoveries that improve our understanding of sperm locomotion and physiological processes to achieve fertilization. In this Review, we discuss technical advances for sperm analysis and provide comprehensive summaries of clinical applications and discoveries enabled by these techniques. Challenges and opportunities to realize high-throughput, non-invasive and high-precision sperm analysis are also discussed.

Clinical application of sperm analysis

Tools for sperm analysis are valuable in the diagnosis and treatment of male factor infertility. Sperm motility, morphology and genetics are important measures of infertility evaluation, and technological advances improve accuracy, efficiency and reduce invasiveness (TABLE 1). Regarding sperm motility, the percentage of motile sperm, straight line velocity and straightness are significantly negatively associated ($P < 0.05$) with time to pregnancy, and increased time to pregnancy indicates a reduction in fecundity[53]. Normal sperm morphology is an important predictor of probability of conception[54,55], with the percentages of morphologically normal sperm significantly different ($P = 0.0002$) between the group that obtained pregnancy (median 5.9%) and the group that did not (median 2.9%)[54]. The DNA fragmentation index is predictive of fertility in couples undergoing IUI, and ICSI is recommended if the DNA fragmentation index exceeds 30%[56,57]. Novel markers have the potential to predict ART outcomes with increased accuracy. For example, the sperm epigenome provides a general view of cellular activity, and abnormal epigenetic patterns such as defective DNA methylation and altered microRNA have been associated with oligozoospermia (low sperm count)[58] and poor pregnancy outcomes[59].

Analysis of sperm motility

Sperm locomotion is generated by the sperm flagellum[60] (FIG. 1), and the flagellum movement is further driven by the axoneme, which is located along the central line of the flagellum. The axoneme consists of a central pair of microtubules that are surrounded by nine pairs of microtubule doublets and nine outer dense fibres,

Table 1 | **Sperm analysis-enabled clinical applications**

Application	Techniques	Refs
Motility and morphology analysis		
Sperm motility measurement	Traditionally performed by manual estimation; computer-aided sperm tracking is more accurate and consistent	33
Sperm morphology measurement	Traditionally performed using fixation and staining that destroys sperm and changes sperm head dimension	73
Non-invasive morphology measurement	DIC imaging to increase sperm contrast, image reconstruction and processing for automated measurement	35
3D morphology measurement	Interferometric phase microscopy by reconstructing a phase map to reflect the actual optical thickness of a sperm	87
Genetic analysis		
DNA fragmentation measurement	SCSA, TUNEL, SCD and comet assay are commonly used but destroy sperm during measurement	245
Non-invasive DNA fragmentation measurement	Raman spectroscopy extracts DNA information from inelastic light scattering by molecular vibrations	126
Chromosomal aberration measurement	FISH uses DNA probes to identify chromosome abnormalities, but can only measure a few chromosomes	16
Genome-wide chromosomal aberration measurement	aCGH and NGS both provide genome-wide screening; NGS has the greatest accuracy	141
Telomere measurement	Quantitative FISH measures the telomeres in a single sperm; real-time PCR has increased sensitivity and efficiency	102,147
DNA methylation analysis	Microarray analysis and NGS for methylation pattern analysis	159,160
Histone modification analysis	Chromatin immunoprecipitation using protein-specific antibodies to identify the DNA–protein complex	163
RNA analysis	Real-time PCR and RNA sequencing for analysis of RNA sequence, LC–MS for analysis of RNA modifications	166,167,170
Sperm sorting and selection		
Sperm selection by motility	Swim-up relies on the active movement of sperm from liquefied semen or a prewashed cell pellet into an overlaying medium	182
Sperm selection by density	In density gradient centrifugation, ejaculate is placed on top of the density media, and after centrifugation, motile sperm are enriched at the bottom of the media	22
Sperm selection by normal morphology	IMSI uses a high-magnification objective to select sperm with normal subcellular structures, but is time consuming	78
Sperm sorting by racing motile sperm inside microchannels	Microfluidic device enables collecting motile sperm at the outlet	185
Using boundary-following behaviour to select sperm with low DNA fragmentation	Microfluidic device with branched microchannels	28
Sperm selection by using fluidic flow to induce rheotaxis	Microfluidic device with fluidic flow and geometric constraint	42,183
Using chemical gradient to select sperm with chemotactic behaviour	Microfluidic device to generate chemical gradient along microchannels	184
Hyaluronic acid as a physiological selector of sperm	PICSI uses a Petri dish with hyaluronic acid coated on it, and hyaluronic acid-containing medium can also be used	29,189
Annexin V used to separate apoptotic sperm	Magnetic activated cell sorting to exclude apoptotic sperm binding with annexin V	30

aCGH, array comparative genomic hybridization; DIC, differential interference contrast; FISH, fluorescence in situ hybridization; IMSI, intracytoplasmic morphologically selected sperm injection; LC–MS, liquid chromatography–tandem mass spectrometry; NGS, next-generation sequencing; PICSI, physiological intracytoplasmic sperm injection; SCD, sperm chromatin dispersion; SCSA, sperm chromatin structure assay; TUNEL, terminal deoxynucleotidyl transferase dUTP nick-end labelling.

forming the 9 + 9 + 2 structure (FIG. 1A and 1B). Dynein attaches to adjacent microtubule doublets and exerts a sliding force between them, resulting in the bending of the flagellum and sperm locomotion[61]. The outer dense fibres contribute to force transmission and add mechanical rigidity along the flagellum[62]. Sperm locomotion is powered by ATP generated by the mitochondria, which are located in the mitochondrial sheath of the midpiece[63]. The motion of the connecting piece (the structure connecting the sperm head and flagellum) is difficult to observe, but the elastic compliance of the connecting piece is hypothesized to be responsible for flagellum beat initiation and the alternating direction of bends propagating down the beating flagellum[64].

Visually tracking a sperm is necessary to analyse sperm locomotion. Tracking sperm trajectories and

measuring sperm motility have important roles in the clinical diagnosis of male factor infertility[65]. The WHO sperm motility parameters (such as curvilinear velocity and linearity, among others) are all calculated from sperm trajectories[10]. To obtain the trajectories of multiple sperm, automated tracking generally includes three steps: image segmentation to obtain the contour and centroid position of each sperm head, linking the position of the same sperm in subsequent image frames (that is, time instances) to obtain the trajectory of each sperm, and calculating sperm motility parameters from the obtained trajectories[66].

As a sperm sample contains a high number of sperm within a field of view under the microscope, a major technical challenge in tracking sperm trajectories is how to accurately distinguish sperm in close proximity (or crossover). Commercial computer-aided sperm analysis systems use the nearest neighbour (NN) or the global nearest neighbour (GNN) algorithms for associating sperm positions at different time points to form a trajectory for each sperm[67]. The NN method assumes the nearest measurement to the tracked sperm to be the correct association. Similarly, the GNN method assumes the association that minimizes the global sum of pair-wise

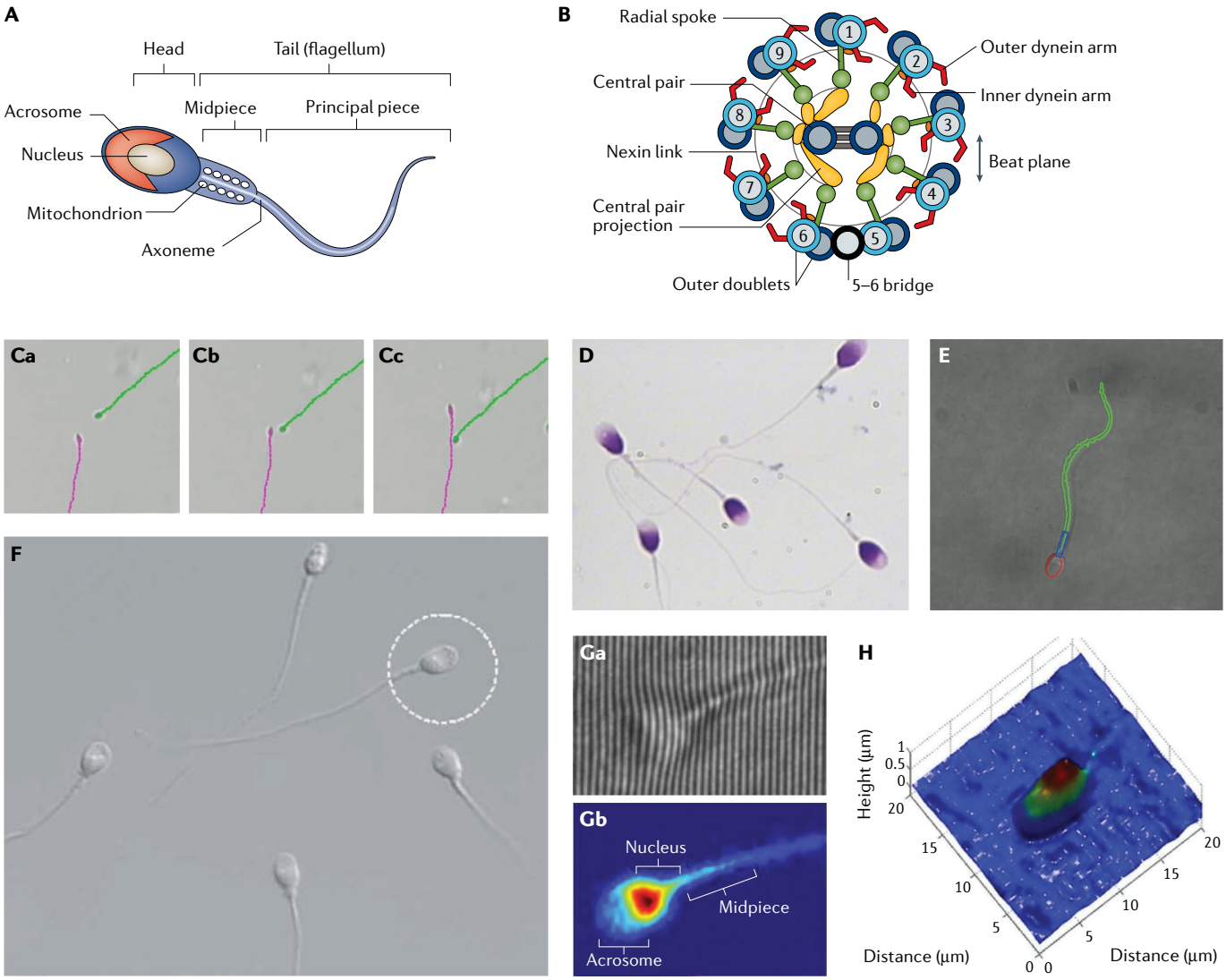

Fig. 1 | **Analysis of sperm motility and morphology. A** | A sperm is composed of a head, a midpiece, a principal piece and an endpiece. For a morphologically normal sperm, an acrosome covers 40–70% of the head area. The acrosome region should contain no large vacuole or no more than two small vacuoles. **B** | The flagellar axoneme consists of a central pair of microtubules that are surrounded by nine pairs of microtubule doublets and nine outer dense fibres. Sliding between the doublets results in the bending of the flagellum and sperm locomotion. The outer dense fibres transmit the force and add mechanical rigidity along the flagellum. **C** | Tracking of two sperm during crossover. **D** | Fixation and staining of a semen smear for morphology analysis. **E** | Automated measurement of live sperm morphology, without invasive staining. **F** | The use of intracytoplasmic morphologically selected sperm injection to select sperm with normal morphology under high magnification. **G** | In interferometric phase microscopy, an interference image is generated by overlaying two beams, one traversing the sample and one reference beam. A phase map is reconstructed to reflect the actual optical thickness of a sperm. **H** | Head height profile of a sperm measured by interferometric phase microscopy. Part **A** is adapted from REF.[246], Springer Nature Limited. Part **B** is reprinted from REF.[21], Springer Nature Limited. Part **D** is reprinted from REF.[73], CC BY 4.0 (https://creativecommons.org/licenses/by/4.0/). Part **F** is reprinted with permission from REF.[247], Elsevier. Part **G** is adapted with permission from REF.[89], Elsevier. Part **H** is reprinted with permission from REF.[88], CUP.

distance to be the correct association[68]. However, both NN and GNN are prone to false association, and tracking mismatch can happen during sperm crossover. To tackle the crossover problem, a joint probabilistic data association filter (JPDAF) method has been developed[69] (FIG. 1C) by modelling the dynamics of sperm movement. The JPDAF method uses the current measurement to enumerate all possible associations and calculates the association probability to effectively distinguish sperm. By incorporating sperm morphology information, the JPDAF method achieved a higher tracking accuracy than that the NN or GNN methods[35] (TABLE 1).

With advances in sperm-tracking algorithms, automated platforms have been developed for quantitative analysis of sperm motility[70,71]. In system validation, correlation coefficients higher than 0.85 between automated and manual grading of sperm motility (rapid, medium, slow and static) were achieved[70]; and correlation coefficients higher than 0.86 were also achieved for the measurement of total motility percentage and progressive motility percentage[71]. These automated systems have potential for improved male infertility diagnosis.

Analysis of sperm morphology

Sperm undergo a series of morphological changes during spermatogenesis, from round spermatid to elongated spermatozoa. Normal sperm morphology indicates normal spermatogenesis that is required for the sperm to develop functions for fertilization and has been positively correlated with fertilization and pregnancy rates[13,14]. A sperm is composed of a head, a midpiece, a principal piece and an endpiece (FIG. 1A). Normal morphology criteria have been defined by the WHO on the basis of observations of sperm recovered from the female reproductive tract[10]: the head should be smooth and generally oval in shape; the acrosome should cover 40–70% of the head area[72]; the acrosome should contain no large vacuole or no more than two small vacuoles that occupy no more than 20% of the sperm head, and the post-acrosomal region should not contain any vacuole[10]; the midpiece should be slender and about the same length as the head, with its major axis aligned with the major axis of the head; residual cytoplasm should not exceed one-third of the head size; the principal piece should be uniform along its length, thinner than the midpiece, approximately 45 μm in length, and should not have a sharp bend or a coil[10].

Conventional morphology analysis is performed by fixation and staining of a semen smear[73] (FIG. 1D). Staining increases the contrast of sperm to improve visualization, but destroys the sperm and makes them unusable for infertility treatment (TABLE 1). Staining also changes the morphometric dimensions of the sperm by either swelling or shrinking the sperm head, according to the osmolarity of the fixatives and stains[74]. To circumvent invasive staining, automated measurement of live sperm morphology has been developed[35]. Differential interference contrast (DIC) imaging has been used to non-invasively enhance sperm contrast; image reconstruction was performed to remove the side illumination effect in DIC imaging, and fuzzy c-means clustering was used to segment sperm from the background[35] (FIG. 1E; TABLE 1).

To select morphologically normal sperm for ICSI treatment, microscope objectives of 20× or 40× are commonly used, but their imaging resolution is insufficient to visualize sperm subcellular structures (such as vacuoles)[75]. Motile sperm organelle morphology examination was developed by using a 100× objective to observe subcellular structures[76,77]. The use of a high-magnification objective in ICSI means that a sperm with normal subcellular structures can be selected and used for intracytoplasmic morphologically selected sperm injection (IMSI) (FIG. 1F; TABLE 1). Studies reported a significantly higher implantation rate (31% versus 20%, $P = 0.007$) and pregnancy rate (46% versus 26%, $P = 0.001$) using IMSI compared with ICSI in men with severe male factor infertility[78,79]. However, no significant difference in clinical outcomes was observed between IMSI and ICSI in other studies[80,81]. Further trials are required to validate the superiority of IMSI over ICSI. Moreover, selecting sperm using IMSI is time consuming; ~2.5 h of searching is required to find sperm to inject ten oocytes[76] as the field of view under 100× magnification is considerably smaller than that under 20× or 40× magnification. Prolonged exposure of sperm to polyvinylpyrrolidone, which is commonly used in ICSI and IMSI, can lead to increased DNA fragmentation[82]. Manual observation is also subjective, leading to inconsistency in sperm selection[83]. Thus, automation techniques have been developed to quantitatively measure sperm morphology under 100× magnification and automatically search for sperm with normal subcellular structures[35,84]. To circumvent the limited field of view under 100× magnification, an automated system was designed to firstly measure motility for all the sperm within the field of view under a low magnification (20×), then a sperm of interest was automatically relocated by the system after switching to a high magnification (100×) for morphology measurement[35]. Image segmentation was performed to extract the sperm contour and measure different subcellular structures such as vacuoles with measurement errors less than 5%[84]. The system has a high efficiency of motility measurement under 20× magnification and provides quantitative morphology measurement under 100× magnification.

Phase contrast microscopy converts phase changes into brightness changes[85] and DIC imaging enhances image contrast by visualizing optical path length changes[86], but they do not reflect actual optical thickness. Interferometric phase microscopy can be used to obtain the 3D morphological information of a sperm[87]. This technique generates quantitative data of the 3D structure of a sperm by overlaying two light beams, one traversing the sample and a reference beam, to produce an interference image. The interference image can then be reconstructed into a phase map to reflect the actual optical thickness (FIG. 1G; TABLE 1). Using interferometric phase microscopy the head height profile of a sperm can be obtained (FIG. 1H). The crater-like appearance of vacuoles can be observed on the sperm head, and the vacuoles indicate chromatin condensation failure and sperm DNA damage[88]. Compact systems of interferometric phase microscopy have also been developed that can be connected to the camera port of a regular

inverted microscope, which is more convenient for clinical use[89].

Analysis of sperm genetics

The sperm head contains packaged chromosomes that contribute half of the genetic material to a fertilized embryo[90]. However, the genetic material in the sperm head is susceptible to damage, including DNA fragmentation, chromosome aberrations and telomere shortening[91]. Analysis of sperm genetic material is important for diagnosing male factor infertility. For example, mutations in *CFAP43* and *CFAP44* can cause male infertility, as the genes are involved in the formation of sperm flagella[92,93]. Mutations in *ARMC2* were found in men with primary infertility and can cause multiple morphological abnormalities of the sperm flagella[94]. Mutations in *SUN5* and *PMFBP1* increase the risk of detachment of sperm heads and tails as these genes are engaged in the formation of the sperm head–tail junction[95,96]. Identifying genetic causes of male infertility has implications for reproductive health and helps to personalize therapies (termed pharmacogenetics)[97].

DNA Analysis. DNA integrity is an important metric of sperm quality[98]. Studies have shown that sperm DNA fragmentation is negatively correlated with fertility[99,100]. High sperm DNA fragmentation can cause embryo arrest, implantation failure, pregnancy loss and congenital malformation[27,101]. The common causes of sperm DNA fragmentation include oxidative stress, abortive apoptosis and aberrant protamine expression[17]. Reactive oxygen species (ROS) are reactive free radicals and are generated by sperm and leukocytes in seminal plasma[17]. Although ROS are involved in tyrosine phosphorylation and are required for sperm capacitation and activation, excessive ROS can overwhelm the antioxidant defence of the sperm, which is termed oxidative stress[91]. Oxidative stress can be caused by an unhealthy lifestyle (such as smoking, excessive alcohol intake, psychological stress and obesity) and environmental factors (such as exposure to pollution, electromagnetic radiation, and heavy metals such as copper and lead)[91]. Intrinsic causes of oxidative stress include testicular infection, varicocele and advanced paternal age[91]. Oxidative stress is treatable by modifying lifestyles and antioxidant supplementation; thus, evaluating the oxidation level in semen is important. Severe oxidative stress is defined as seminal ROS levels >35 relative light units/s per million sperm using a chemiluminescence assay[102]. Several biomarkers are also commonly used to evaluate oxidative stress, including 8-hydroxy-deoxyguanine (8-OHdG), isoprostane and malondialdehyde[103]; among them, 8-OHdG is the most widely used and is highly mutagenic, with its level positively correlated with male infertility[104]. It can cause germline mutations and lead to certain genetic disorders such as Huntington disease and Marfan syndrome and cancers such as leukaemia and retinoblastoma in the resulting children[105]. A threshold of 65.8% of 8-OHdG-positive sperm cells was determined to discriminate sperm parameter alterations, such as leukocytospermia, by quantifying human sperm DNA oxidation with an anti-8-OHdG antibody[106]. However, the sperm were fluorescently labelled and, therefore, not usable for infertility treatment, but the assay can be used for the diagnosis of male infertility associated with oxidative stress.

Another cause of DNA fragmentation is abortive apoptosis[107]. Apoptosis helps with the removal of damaged or defective sperm during spermatogenesis, but sperm that initiate apoptosis can fail to complete the process owing to, for example, incomplete activation of the endogenous nuclease and lack of synchronization between apoptosis and spermatogenesis[107]. Abortive apoptosis causes sperm with DNA damage to be present in the ejaculate. DNA fragmentation is also caused by aberrant protamine expression[108]. During normal spermatogenesis, histone is replaced with protamine[109]. Aberrant protamine expression with incomplete replacement leads to abnormal chromatin packaging, making the DNA more susceptible to oxidative attack and, therefore, fragmentation[109].

DNA fragmentation can be measured using the SCSA, in which flow cytometry is used to measure the susceptibility of sperm nuclear DNA to acid-induced denaturation by quantifying the metachromatic shift[15] (TABLE 1). Sperm with fragmented DNA fluoresce red in colour and sperm with normal DNA fluoresce green (FIG. 2A) after acridine orange staining. Thus, the SCSA can be used to detect the metachromatic shift rapidly and accurately, providing high statistical robustness and interlaboratory reproducibility[101]. The clinical threshold of the red:green ratio for a normal sperm sample is 30%, meaning that samples with up to 30% of detectable DNA-damaged sperm are considered normal[110]. Terminal deoxynucleotidyl transferase dUTP nick end labelling (TUNEL) can also be used to detect DNA damage in sperm. This technique uses fluorescent nucleotides to detect the free end of DNA[111]. Standard fluorescence microscopy or flow cytometry is used to analyse the sample and fluorescence intensity increases with the number of single-stranded or double-stranded DNA breaks (FIG. 2B; TABLE 1). A threshold for TUNEL assay to distinguish between fertile and infertile men was determined to be 20% of sperm with detected DNA fragmentation[112]. However, the TUNEL assay lacks standardization and consistency[113]. The robustness and accuracy of the TUNEL assay can be improved by relaxing the sperm chromatin structure with dithiothreitol before fixation[114] and by analysing the results with a flow cytometer instead of a fluorescence microscope[115].

The sperm chromatin dispersion test is based on the concept that sperm with fragmented DNA do not produce the characteristic halo of dispersed DNA loops[116] (TABLE 1). The dispersed loops are observed in sperm with non-fragmented DNA following acid denaturation and removal of nuclear proteins (FIG. 2C)[117]. Halos can be observed via bright-field microscopy if staining is done with an eosin and azure B solution or via fluorescence microscopy if DNA-directed fluorochromes are used. Because the shape of a sperm halo is distinct, sperm chromatin dispersion has small interobserver variation and the consistency between its manual and digital image analysis is high[117]. Single-cell gel electrophoresis

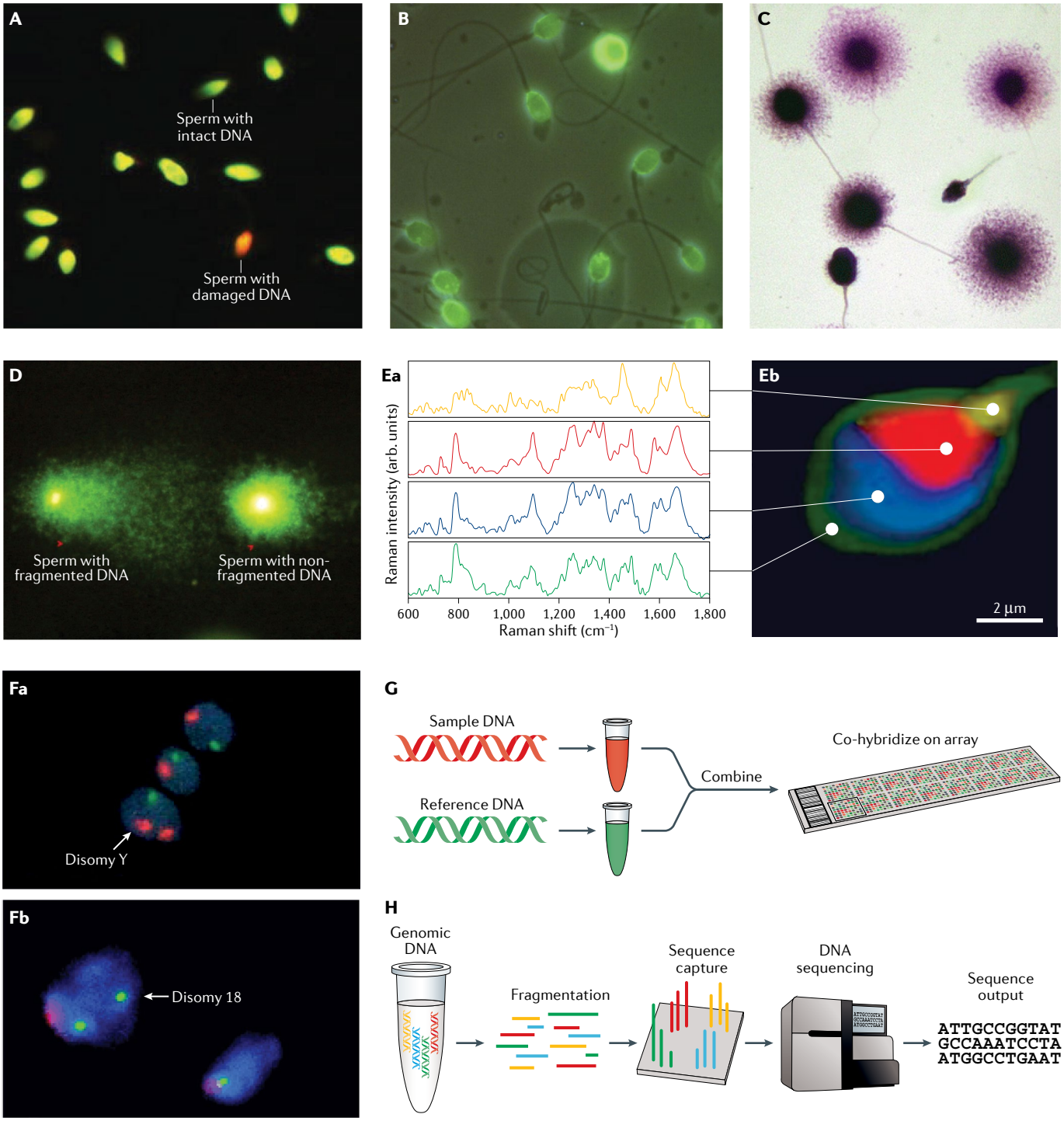

Fig. 2 | **Analysis of sperm genetics. A** | The sperm chromatin structure assay, in which sperm with damaged DNA fluoresce red and those with normal DNA fluoresce green. **B** | Using terminal deoxynucleotidyl transferase dUTP nick-end labelling, green fluorescence indicates the presence of DNA fragmentation. **C** | The sperm chromatin dispersion test, in which sperm with fragmented DNA do not produce the characteristic halo of dispersed DNA loops. **D** | In the comet assay, DNA fragments form the comet tail; DNA fragmentation of a sperm is indicated by its comet tail length and moment. **E** | Raman spectra acquired from cell membrane (green line), acrosomal vesicle (blue line), nucleus (red line) and midpiece (yellow line). The spectra are used to reconstruct the false colour Raman image. **F** | The fluorescence in situ hybridization test uses chromosome-specific DNA probes to measure sperm aneuploidy. The image shows a sperm nucleus exhibiting disomy for chromosomes Y (red) and disomy for chromosomes 18 (green). **G** | In array comparative genomic hybridization, sperm DNA from a patient and a normal control are labelled using fluorescent dyes and mixed together and hybridized on a microarray. **H** | In next-generation sequencing, DNA is first fragmented into stretches of 50–500 nucleotides, and billions of the DNA fragments are then captured in an array and analysed in a single reaction. Part **A** is adapted from REF.[248], Springer Nature Limited. Part **B** is reprinted from REF.[249], Elsevier. Part **C** is reprinted from REF.[250], Springer Nature Limited. Part **D** is reprinted from REF.[101], Springer Nature Limited. Part **E** is adapted from REF.[125], CC BY 4.0 (https://creativecommons.org/licenses/by/4.0/). Part **F** is reprinted with permission from REF.[251], OUP. Part **G** is reprinted from REF.[252], Springer Nature Limited.

(also known as the comet assay) quantitatively measures DNA fragmentation of individual sperm[118]. In this assay, sperm are embedded in agarose gel on a microscope slide, and after lysis their DNA is stained. By performing electrophoresis, fragmented DNA from damaged sperm chromatin migrates from the sperm head[119]. The fluorescent image of the sperm after electrophoresis shows a comet-like shape with a tail (FIG. 2D; TABLE 1). The intensity and the length of the comet tail reflect the number of DNA breaks. The alkaline comet assay (which uses alkaline electrophoresis solution) can distinguish single-stranded and double-stranded DNA breaks, but neutral comet assay only detects double-stranded DNA breaks[120,121]. Men with sperm DNA fragmentation higher than 25% measured using the alkaline comet assay were at a high risk of having male factor infertility[122]. Double-stranded DNA fragmentation in sperm measured using the neutral comet assay is associated with recurrent pregnancy loss[123]. However, the labour-intensive protocol of the comet assay is the main drawback that limits clinical application.

The staining methods for sperm DNA fragmentation measurement are invasive. The measured sperm are killed during fixation and staining and, therefore, are unusable for treatment. Raman spectroscopy is a non-invasive approach of measuring DNA fragmentation[124]. In Raman spectroscopy, information on DNA and protamine is extracted directly from the inelastic light scattering induced by their molecular vibrations[125] (FIG. 2E; TABLE 1). The intensities of DNA-specific Raman spectra positively correlated with the degree of DNA packaging within the chromatin[126]. The effect of hydration conditions on the Raman spectrum of sperm DNA has been studied by comparing the spectra of sperm in dry conditions and aqueous media. The results revealed that DNA damage was only observed in air-dried sperm but not in sperm in aqueous media using Raman spectroscopy[127]. Thus, the application of Raman spectroscopy in living sperm analysis requires further investigation. Moreover, Raman spectroscopy requires specialized set-up and staff training, and might not fit into the workflow of typical clinical settings.

Techniques have also been developed that correlate sperm morphology with DNA fragmentation so that a sperm's DNA integrity can be non-invasively predicted. By correlating bright-field images of sperm with their fluorescence images after acridine orange staining, a predictive model based on logistic regression was established that had an accuracy of 0.827 (REF.[128]). The model can be used to evaluate the DNA fragmentation of a sperm based on its morphology[128]. Sperm morphology assessed by interferometric phase microscopy was also correlated with DNA fragmentation, showing a significant difference ($P < 0.05$) in interferometric phase microscopy-based parameters among groups of sperm with different DNA fragmentation levels[129]. With the advent of deep learning, raw images can be used to train the prediction models[130], which might find important features humans miss and improve the prediction accuracy. A deep convolutional neural network was trained based on a dataset of 1,000 sperm, and achieved a moderate correlation of 0.43 between sperm bright-field image and DNA quality[130].

Chromosomal analysis. Sperm chromosome aberrations are common in men who are infertile; 2–14% infertile men have some degree of chromosomal aberration, and increasing chromosomal aberration correlates with increasing severity of infertility[131,132]. Numerical chromosomal aberrations, called aneuploidy, and structural aberrations are associated with recurrent pregnancy loss and birth defects[133]. The standard technique for measuring genetic heterogeneity in individual sperm within a population is FISH. The FISH assay uses chromosome-specific DNA probes to obtain a karyotype that enables identification of variations in chromosomal number or structure[134] (TABLE 1). The chromosome-specific DNA probes are labelled with fluorescent compounds. After induced sperm decondensation, these probes bind to the target positions of specific chromosomes[16] (FIG. 2F). However, FISH only measures aneuploidy frequencies for a few chromosomes in sperm as it typically uses dual colour or triple colour probes for sperm testing. Multicolour FISH has been developed, but it has a limited resolution and is not used for genome-wide screening[135].

Molecular testing techniques have been developed to measure genome-wide aberrations. Array comparative genomic hybridization (aCGH) uses designed probes to detect thousands of DNA targets for genome-wide screening[136] (TABLE 1). In aCGH, sperm DNA of a patient and a normal control are labelled using fluorescent dyes and mixed together and hybridized on a microarray[137] (FIG. 2G). aCGH provides a higher resolution than FISH as its probes are several orders of magnitude smaller than chromosomes[138]. Testing with aCGH showed that sperm from men undergoing chemotherapy had a higher rate of chromosome aberration than healthy donors (23.8% versus 7.8%)[139]. The technique can be used for genome-wide sperm analysis, especially in patients at an increased risk of sperm genetic abnormalities, such as men with advanced age, men treated with chemotherapy and couples with repeated miscarriages.

NGS currently provides the highest accuracy for chromosomal aberration measurement[140]. In NGS, DNA is first fragmented into stretches of 50–500 nucleotides and billions of these DNA fragments are then captured in an array and analysed in a single reaction (FIG. 2H; TABLE 1). The sequence of each DNA fragment is mapped back and compared with the reference human genome[141]. NGS was performed on sperm from an infertile group of men and a fertile group of men; the infertile group was found to have an overall aneuploidy rate of 8.6%, significantly higher than the 4.0% in the fertile group ($P < 0.00001$)[142]. In the infertile group, 17 genes engaged in fertilization and embryo development with the highest mutation rate were identified[142].

Telomere analysis. The telomere is a region of the nucleotide sequence at each end of a chromosome and protects the ends of the chromosome[143]. The telomere has an important role in maintaining chromosomal

stability and cell viability[144]. Sperm telomere length is shorter in infertile men[145], and is significantly positively correlated with sperm count ($P < 0.001$) and the quality of early embryonic development after IVF ($P < 0.001$)[146]. Analysis of telomere length is usually achieved using quantitative FISH (qFISH) and real-time PCR (rtPCR) (TABLE 1)[147]. In qFISH, a telomeric sequence is hybridized with a specific peptide nucleic acid probe, and the telomere length is measured under a fluorescence microscope[147]. This technique can measure the telomere length in a single sperm or even a single chromosome. Using qFISH, sperm exposed to high concentrations of hydrogen peroxide during incubation were found to have reduced telomere length[148]. This observation indicates that oxidative stress can be a cause of telomere shortening. Paternal age also affects telomere length; men aged >35 years had a significantly longer sperm telomere length than men aged <35 years ($P < 0.05$)[149].

In quantitative rtPCR, the relative mean telomere length is determined by comparing the quantity of telomere DNA with the quantity of reference gene such as *36B4* (REF.[102]). rtPCR has greater efficiency and sensitivity than qFISH, although it only provides the mean telomere length of a sperm sample and cannot measure the telomere length of individual sperm[147]. Using rtPCR, sperm telomere length was found to be significantly negatively correlated with aneuploidy ($P = 0.037$)[150]. Among 51 sperm samples being analysed for IVF, 17.6% had atypical telomere length and none of these resulted in pregnancy, but the remaining samples with normal telomere length achieved a pregnancy rate of 35.7%[150]. This observation suggests that sperm telomere length can have a high predictive power for IVF outcomes, which requires further investigation in a larger sample size.

Given the relationship between sperm telomere length, male factor infertility and ART outcomes, selecting sperm with normal telomere length is desirable for infertility treatment. Sperm preparation techniques can help to select sperm with longer telomeres. For instance, the average length of sperm telomeres was significantly longer after density gradient centrifugation ($P < 0.001$) or swim-up ($P = 0.011$) than the length of sperm telomeres in raw semen, although no significant difference was found between the two procedures[151]. For sperm selection for ICSI, a sperm is not usable after molecular analysis of telomere; thus, associating morphological parameters with telomere length might provide a non-invasive approach to predicting a sperm's telomere length[152].

Epigenetic analysis. Sperm epigenetics is important for the regulation of spermatogenesis and early embryo development[153]. Sperm epigenetic modifications include DNA methylation, histone modification and non-coding RNA generation[153]. Abnormal sperm epigenetic patterns, such as defective methylation of imprinted genes, are associated with oligozoospermia[58] and poor embryogenesis[154]. Significantly different epigenetic patterns ($P < 0.05$) were found between two groups of sperm samples that led to different blastocyst quality in IVF cycles. Genes involved in embryonic development were less methylated ($P < 0.05$) and microRNAs were altered ($P < 0.05$) in sperm from the poor blastocyst group[155]. Thus, information regarding sperm epigenetics can provide insight into spermatogenetic disorders and help to predict the ART outcomes.

Analysis of DNA methylation has two steps: recognition of methylated DNA and methylation pattern analysis[156]. The recognition of methylated DNA is usually achieved by bisulfite conversion[156,157] and methylated DNA immunoprecipitation[158]. Bisulfite treatment converts unmethylated cytosine into uracil residues and does not affect methylated cytosine[157]. Methylated DNA immunoprecipitation uses immunoprecipitation with antibodies that specifically recognize methylated cytosine[158]. The methylation pattern is then analysed using a microarray[159] or NGS (TABLE 1)[160,161]. In microarray analysis, target DNA is labelled with a fluorescent dye for hybridization. The signal intensity of each hybridized probe is used to quantify DNA methylation patterns[159]. However, microarray design requires prior knowledge of the genomic features, which hampers the discovery of undefined genomic features. Cross-hybridization between similar sequences also restricts microarray analysis to the non-repetitive fraction of genomes[162]. NGS addresses these two limitations by not requiring prior knowledge of genomic features and directly sequencing DNA without hybridization[160]. Using microarrays and NGS, elevated levels of DNA methylation were found in poor-quality sperm samples (concentration $<5 \times 10^6$/ml or total motile sperm count $<10^7$)[163], and an altered DNA methylation pattern was characterized in sperm from patients displaying abnormal embryogenesis[164].

Histone modification analysis is usually performed using chromatin immunoprecipitation (ChIP)[165,166] (TABLE 1). ChIP identifies the binding sites for a given DNA-associated protein by using protein-specific antibodies to immunoprecipitate the DNA–protein complex[165]. As the majority of the DNA is bound to protamines rather than histones in sperm, only a small amount of DNA is available after isolation, and whole-genome amplification can be performed after ChIP to increase the amount of DNA available for downstream analysis[166]. Nucleosomes are widely replaced by protamine in sperm; thus, the epigenetic contribution of sperm to embryo development was considered limited. However, the use of ChIP on human sperm revealed that histones are retained at many loci that are important for embryo development, including transcription factors and signalling pathway components[167].

RNA in sperm affects embryo development by modifying gene expression starting from fertilization[168]; it also contributes to stabilizing the nuclear envelope and marking the DNA sequences that stay bound to histones, which is important for embryogenesis[169]. Thus, RNA might be a marker of male infertility. The commonly used RNA analysis techniques are rtPCR[170], RNA sequencing (RNA-seq)[171] and liquid chromatography–tandem mass spectrometry (LC–MS)[172] (TABLE 1). rtPCR can qualitatively detect gene expression through the creation of complementary DNA (cDNA) transcripts from RNA and quantitatively measure the amplification of cDNA using fluorescent probes[170]. However, rtPCR can only analyse RNA with known sequences

because it relies on predesigned probes. RNA-seq performs high-throughput sequencing with NGS of cDNA to obtain information about RNA content[173]. This technique has greater efficiency than rtPCR and can analyse RNA with unknown sequences[171]. Using rtPCR and RNA-seq, abnormally elevated protamine mRNA retention in sperm was found to be associated with protamine deficiency in sperm and male factor infertility[174]. Sperm mRNA was discovered to be delivered to the oocyte at fertilization[175] and have a considerable role in embryo development[176,177]. In mice, mRNA injection into oocytes led to epigenetic changes and induced a heritable phenotype[176], showing that mRNA can influence embryo development through epigenetic modifiers[169]. mRNA encoding proteins such as clusterin transferred by the human sperm to the oocyte are involved in cell–cell interaction, lipid transportation and membrane recycling[175]. LC–MS is currently the only technique capable of comprehensively characterizing RNA modifications[172]. RNA modifications are involved in the transcriptional and epigenetic regulation of various biological processes including spermatogenesis[178]. LC–MS analyses RNA by separating and measuring mass:charge ratios of molecules to deduce molecular structure and sequence. Using LC–MS, RNA modifications present in transfer RNA-derived small RNAs (tsRNAs) were found to increase RNA stability in mouse sperm. Sperm tsRNAs have also been found to contribute to intergenerational inheritance of a metabolic disorder[179]. Further research on sperm tsRNAs could help to improve our understanding of human diseases caused by paternal epigenetics.

The clinical implementation of genetic profiling of sperm would help to assess spermatogenetic disorders[58], male infertility[99], sperm contribution to normal embryogenesis[156] and ART success[27]. The analysis of sperm genetics has been advanced by techniques such as NGS, rtPCR and RNA sequencing, but most of the approaches to sperm genetic analysis destroy sperm and make them unusable for infertility treatment. To select sperm without genetic defects, non-invasive techniques have been developed to either directly measure (such as Raman spectroscopy)[126] or predict a sperm's genetic quality[128–130]. The prediction models are based on the correlation between sperm morphology assessed non-invasively and the genetic quality, and are easier to integrate into clinical workflow than Raman spectroscopy as they do not require additional setup.

Sperm isolation and selection

Sperm analysis has considerable diagnostic value and also enables the development of new techniques for sperm isolation and selection (TABLE 1). Sperm isolation is required for infertility treatment, as sperm with the highest fertilization potential need to be separated from the raw semen. The motility[180] and DNA integrity[181] of isolated sperm are substantially better than those of the raw semen. Various methods have been developed for sperm isolation. Swim-up is an easy-to-perform and cost-effective method that relies on the active movement of sperm from liquefied semen or a prewashed cell pellet into an overlaying medium[182]. The supernatant containing motile sperm can then be collected. The use of swim-up is limited to ejaculates with high sperm count and motility[182]. Density gradient centrifugation (DGC) is another commonly used method of sperm isolation. In DGC, the ejaculate is placed on top of the density media, and the density increases from the top to the bottom of the density media, either continuously or discontinuously[182]. After centrifugation for 15–30 min, motile sperm are enriched at the bottom of the media. DGC is suitable for sperm isolation in ejaculates with low sperm concentration such as oligozoospermic samples[22].

Swim-up and DGC are widely used in fertility clinics, but these traditional methods of sperm separation cannot select sperm with high DNA integrity[22]. To select optimal sperm for infertility treatment, several techniques have been developed. Specially designed microfluidic devices are able to sort sperm with geometric constraints and various stimuli[183,184]. Most of the devices developed use passive selection that relies on sperm locomotion. For example, a microfluidic device was designed to achieve sperm sorting by racing sperm inside microchannels and collecting motile sperm at the outlet[185]. With an incubation time of an hour and a channel length of 20 mm, the curvilinear velocity of sperm at the outlet was 4.7-fold higher than that of sperm at the inlet (FIG. 3a; TABLE 1). Motile sperm were found to preferentially accumulate near boundaries owing to the hydrodynamic interaction with the surface[47], and boundaries are common in the female reproductive tract such as the fallopian tube with folded epithelium[186]. Motile sperm were collected microfluidically based on their boundary-following behaviour. Sperm-exhibiting boundary-following characteristics were found to have reduced DNA fragmentation[28] (FIG. 3b; TABLE 1). Microfluidic devices that use active sperm selection have also been developed, such as using fluidic flow and chemical gradient. For instance, by controlling the flow rate of sperm medium, rheotaxis zones were created in front of corral structures inside a microfluidic channel. Sperm with upstream swimming behaviour were isolated inside the corral structures (FIG. 3c; TABLE 1), and the effect of flow rate on the velocity of isolated sperm was investigated[187]. As the flow rate increased from 0.6 ml/h to 1.8 ml/h, the minimum velocity of the isolated sperm increased from 43 μm/s to 55 μm/s. The isolated sperm were demonstrated to be 100% progressively motile. A device mimicking narrow junctions inside the female reproductive tract was developed using fluidic flow and geometric constraint to prevent sperm with low motility from advancing through the constraint[183] (FIG. 3d). Another microfluidic device was designed by exploiting sperm chemotaxis, in which sperm swim against a chemical gradient[188]. Chemotaxis was induced by progesterone, a chemoattractant secreted by cumulus cells in the female reproductive tract[184] (TABLE 1). Sperm with normal morphology and reduced DNA fragmentation were selected using this device.

Hyaluronic acid surrounds an oocyte in vivo, and sperm that bind with hyaluronic acid are shown to be mature, viable and have unreacted acrosome status[189]. Thus, hyaluronic acid has been used as a physiological

sperm selector (TABLE 1). Sperm binding with hyaluronic acid were found to be all viable[189] (identified by staining as green; FIG. 3e). Currently, two tools are commonly used for incorporating hyaluronic acid into ART: a physiological intracytoplasmic sperm injection (PICSI) dish[31] and a commercially available hyaluronic acid-containing medium[29]. In PICSI, the petri dish includes areas of immobilized hyaluronic

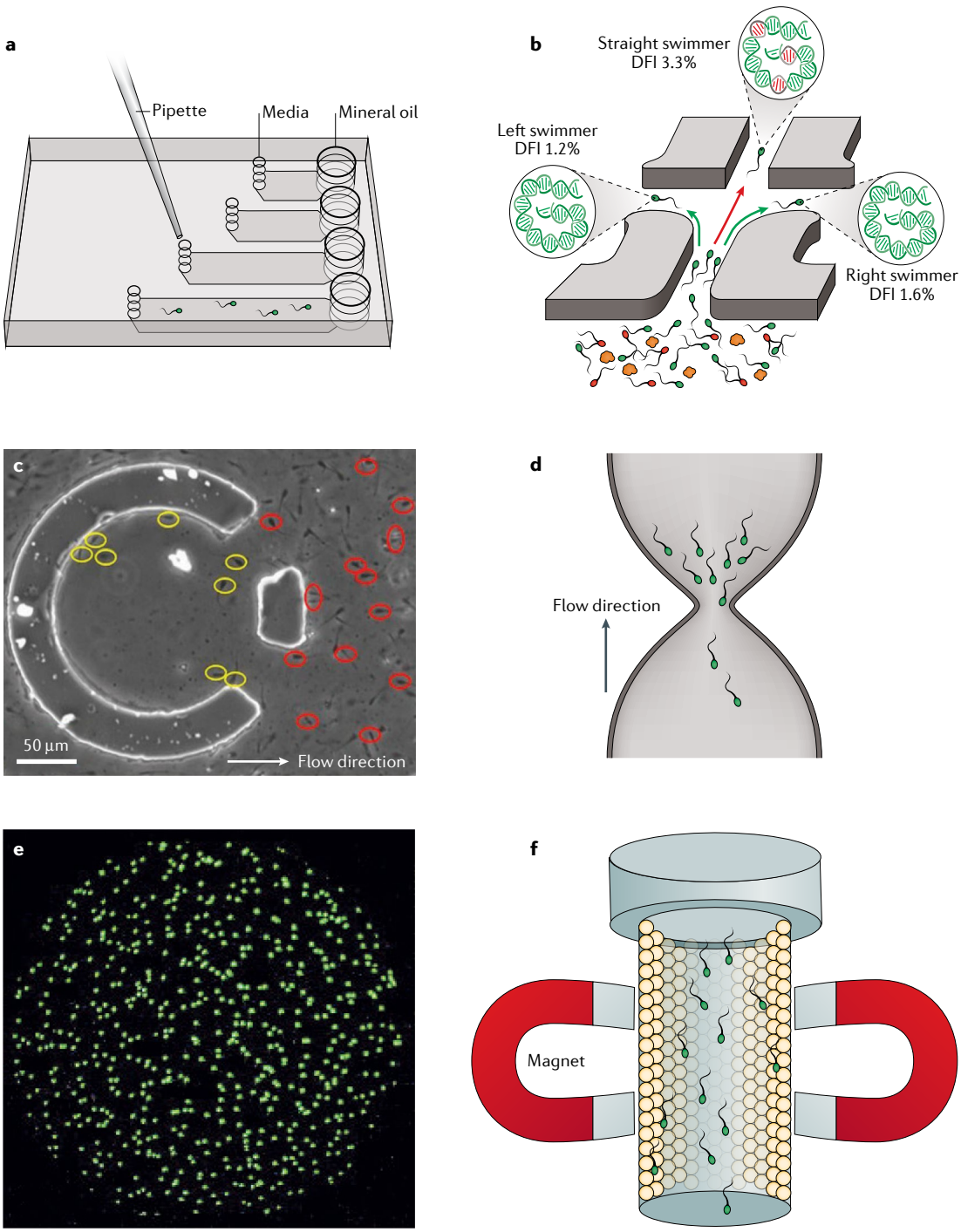

Fig. 3 | **Analysis-enabled sperm selection. a** | A microfluidic device to sort sperm by exhaustion of sperm inside microchannels. **b** | The left-swimming and right-swimming sperm had a lower DNA fragmentation index (DFI) than the straight-swimming sperm in a microfluidic device. **c** | Corrals inside a fluid channel are used to induce rheotaxis to isolate motile sperm. Sperm with upstream swimming behaviour are indicated with red ovals, whereas the isolated sperm are indicated with yellow ovals. **d** | A representation of a device with narrow junctions using fluid flow and geometric constraint to isolate sperm. **e** | The sperm that bind with hyaluronic acid are all viable and stain green. **f** | Using annexin V, apoptotic sperm are separated from non-apoptotic sperm using magnetic-activated cell sorting. Part **a** is reprinted with permission from REF.[185], Wiley. Part **b** is reprinted with permission from REF.[28], RSC. Part **c** is reprinted with permission from REF.[42], PNAS. Part **e** is reprinted with permission from REF.[189], Elsevier. Part **f** is reprinted from REF.[22], Springer Nature Limited.

acid where mature sperm can bind, and the binding sperm are selected for ICSI use[31]. To use hyaluronic acid-containing medium, a droplet with a suspension of sperm was connected with a pipette tip to a droplet of hyaluronic acid-containing medium. After incubation, sperm bound to hyaluronic acid in the junction zone were selected[29]. Compared with regular ICSI, the sperm selected by using hyaluronic acid-containing medium showed significantly reduced DNA fragmentation ($P < 0.001$). However, the improvement in embryo quality and implantation rate was not significant ($P > 0.05$)[29]. For PICSI, a study involving 16 assisted reproduction units in the UK reported that the live birth rate of PICSI was not significantly different from that of standard ICSI ($P = 0.18$)[31]. Thus, the use of PICSI and hyaluronic acid-containing medium has not become widespread and still requires further investigation.

Expression of apoptotic markers in sperm is associated with an increased likelihood of DNA damage and poor morphology[190]. Annexin V is a calcium-dependent phospholipid-binding protein that has a high affinity for phosphatidylserine (an apoptotic marker)[191]. Apoptotic sperm can be separated from non-apoptotic sperm using annexin V and magnetic activated cell sorting[30] (MACS; FIG. 3f; TABLE 1). Sperm separated using MACS showed increased normal morphology[30]. Furthermore, the use of MACS-sorted sperm also resulted in increased pregnancy rates ($P = 0.004$) when compared with DGC and swim-up techniques, but no significant differences ($P > 0.5$) were found in implantation and miscarriage rates[192]. This observation suggests that MACS can improve pregnancy rates when used for sperm selection in ART. Notably, besides sperm isolation and selection, methods of improving sperm quality are also important for male infertility treatment. Lifestyle modifications, hormone therapies, surgery to manage varicoceles and antioxidant therapies could all improve fertility[103,193]. In summary, the analysis of sperm motility, morphology, and genetics are the basis of male infertility diagnosis, and aid in the selection of optimal sperm for infertility treatment (TABLE 1).

Sperm analysis for discovery

Sperm analysis has enabled important discoveries about sperm locomotion and behaviour as well as their subcellular and molecular structures. These discoveries improve our understanding of sperm motion and guidance within the female reproductive tract and enable various physiological processes, such as capacitation and acrosome reaction, to be delineated (TABLE 2).

Analysis of locomotion and behaviour

Sperm locomotion is driven by its flagellum; thus, flagellum tracking is required for studying sperm locomotion and behaviour. Sperm flagellum tracking differs from measurement of sperm trajectories, which only tracks a single point (the centroid of the sperm head), in that it typically requires the position of all points along the centreline of the sperm flagellum to be obtained. The challenge for sperm flagellum tracking is the low imaging contrast of the flagellum owing to its small size (<1 μm diameter[61]). Hence, image contrast enhancement is required in flagellum tracking (FIG. 4). For example, the current frame of image and history images of the sperm flagellum have been used to generate an image with enhanced contrast, by summing the absolute differences between consecutive greyscale image frames[194]. To segment the sperm flagellum, the sperm head centroid was used as a starting point and a Kalman predictor estimated the next region around the sperm flagellum. In the region, image contrast was enhanced by history images[194], and a point on the sperm flagellum was located. Then, the prediction and image enhancement was repeated throughout the sperm flagellum to obtain its centreline[195]. Machine learning can also be used for image enhancement; a machine learning-based algorithm has been developed to enhance image contrast three dimensionally for flagellum tracking[196]. Within the 3D image stack the probability of each pixel belonging to the sperm flagellum was predicted using a classifier and set as the pixel value in the contrast-enhanced image[196] (FIG. 4A).

Quantitative analysis of sperm flagella enabled the discovery that a superposition of two bending waves with a fundamental frequency and its second harmonic travels down the flagellum, and this pattern is characteristic of flagellar beating in sperm (FIG. 4B; TABLE 2). The increase in intracellular Ca^{2+} leads to increased intensity of the second harmonic wave, and sperm navigate by adjusting the phase shift (the difference in locations within wave cycles) between the two harmonics[197]. Sperm velocity was found to be proportional to its flagellar beating amplitude, by flagellum tracking on contrast-enhanced images[194]. Tracking of sperm flagella by high-speed imaging (250 Hz) also provided experimental evidence of the resistive force theory[198], a theory suggesting that a propagating flagellar wave produces a propulsive thrust that is balanced by the drag on the sperm head[199]. Experiments on sperm rheotaxis showed that sperm changed their swimming direction when exposed to fluid flow to swim upstream against the flow[200]. Sperm flagellar beating amplitude and asymmetry both remained unchanged while the sperm turned during rheotaxis (FIG. 4C; TABLE 2), providing evidence that rheotaxis is a passive physical process governed by fluid mechanics instead of an active flow-sensing process[200]. Flagellar beat in 3D was constructed by first tracking the flagellum in a 2D plane and then estimating the z position from the width of intensity maxima along the flagellum. The results revealed that rheotaxis turning was independent of the flagellar rolling motion and the chirality of flagellar beat (FIG. 4D; TABLE 2); instead, the asymmetry of the midpiece determined the direction (left-turning or right-turning) of rheotaxis turning[201].

Emerging microscopy methods have been used to analyse sperm behaviours. Using total internal reflection fluorescence microscopy, which selectively illuminates the fluid–substrate interface within one micron of a surface, a 2D slithering swimming mode of sperm was observed (TABLE 2)[46]. In this swimming mode, bovine sperm head and flagellum were confined to a 2D plane within 1 μm of the substrate with no rotation (FIG. 4E), different from the 3D swimming mode in which the

Table 2 | **Sperm analysis-enabled discoveries**

Discoveries	Techniques	Ref.
Locomotion and behaviour		
Sperm flagellar beat consists of two bending waves and sperm navigate by adjusting the phase between the two harmonics	Flagellum tracking	197
Sperm flagellar beating amplitude and asymmetry remained unchanged during rheotaxis; thus, rheotaxis is a passive physical process	Flagellum tracking	200
Rheotaxis turning was independent of the flagellar rolling motion and the chirality of the flagellar beat, but determined by the asymmetry of the midpiece	Flagellum beat reconstruction	201
Sperm exhibit a 2D slithering swimming mode near boundaries	TIRF	46
Opsin proteins located on the sperm membrane function as a thermosensor in sperm thermotaxis	TIRF	202
5% of sperm swim in helices and the majority prefer right-handed helices	Digital holography	44
Sperm swimming speed is positively correlated with spinning speed in 3D, and 100% of sperm show right-handed spin along the head axis	Digital holography	34
Human and horse sperm exhibit a 3D swimming pattern of chiral ribbons. 1.7% of human sperm but 27.3% of horse sperm exhibit chiral ribbons	Digital holography	45
Sperm follow boundaries within microchannels	Microfluidics	47
Corner-swimming sperm dominate with concentrations as high as 200-fold compared with sperm in the centre of the channel	Microfluidics	186
Structure and molecules		
Mitochondria are helicoidally distributed around the axoneme within the midpiece	SNOM	210
CatSper channels are normally distributed in linear quadrilateral domains along the flagellum	STORM	48
In the midpiece, actin forms a double helix that accompanies mitochondria with a periodicity of 244 nm	STORM	216
CD46, a membrane cofactor protein, undergoes dynamic reorganization during the acrosome reaction	STED	218
SUN4, a spermatid nuclear membrane protein, is essential for nuclear remodelling in spermiogenesis	SIM	223
ABHD2 binds to progesterone and activates CatSper channels by removing CatSper inhibitor 2AG	Immunostaining	225
Tyrosine phosphorylation is negatively regulated by Ca^{2+} influx and is part of the signal transduction pathway for capacitation	Immunostaining	226
Ubiquitin is a biomarker for identifying abnormal sperm	Immunostaining	50
Chaperone protein HSPA2 is a biomarker of human sperm maturation	Immunostaining	52
55 sites of phosphorylation and extent of phosphorylation of 42 phosphopeptides were identified during capacitation	Mass spectrometry	229
Protein modification is an important mechanism in sperm maturation based on the discovered peptide residues	Mass spectrometry	231
ECM1 can distinguish obstructive azoospermia from normal spermatogenesis, and TEX101 can further differentiate distinct subtypes of non-obstructive azoospermia based on the cut-off values of expression	Mass spectrometry	232
25-hydroxycholesterol expression is a biomarker of normal sperm	Mass spectrometry	233

2AG, 2-arachidonoylglycerol; ABHD2, abhydrolase domain-containing protein 2; ECM1, epididymis-expressed extracellular matrix protein 1; HSPA2, heat shock protein family A (Hsp70) member 2; SIM, structured illumination microscopy; SNOM, scanning near field optical microscopy; STED, stimulated emission depletion microscopy; STORM, stochastic optical reconstruction microscopy; TEX101, testis-expressed protein 101; TIRF, total internal reflection fluorescence microscopy.

sperm head rotates and the flagellar propulsion is helical[46]. The slithering swimming was also observed in human sperm but only for viscosities over 20 mPa·s. Strong transverse components of human sperm's flagellar wave at low viscosities (<20 mPa·s) inhibited the slither swimming mode. Under increased viscosity, the transverse components were dampened, leading to slither swimming[46]. The 2D slither swimming mode suggests a surface-based sperm migration strategy near the wall of the fallopian tube, where the viscosity of mucus is over 200 mPa·s[46]. Total internal reflection fluorescence microscopy was also used to show that opsin proteins are located on the sperm membrane and function as thermosensors in sperm thermotaxis. Thermotaxis is one of the mechanisms that guide sperm to the fertilization site and regulates sperm swimming direction changes according to a temperature gradient[202] (TABLE 2). Opsins were previously found to act as photosensors in

vision, and this study showed that they also function as thermosensors in sperm.

Digital holography has also been applied to analyse sperm behaviour. This technology numerically reconstructs the phase and amplitude of a sperm's optical wavefront[203]. A large depth of field (for example, 0.5–1.0 mm) can be observed without physically realigning the optical focus by numerically refocusing 2D images on different planes, enabling simultaneous observation of a high number of sperm[204] (FIG. 4F). Digital holography was used to simultaneously track >1,500 human sperm in 3D and showed that ~4–5% of motile sperm swim in well-defined helices[44]. Among these helical-swimming sperm, the majority (90%) showed right-handed helices (TABLE 2). Further investigation of this distinct swimming behaviour can help understanding of sperm navigation inside the female reproductive tract[205]. Fast-swimming sperm also spin fast in 3D, and 100% of the sperm showed right-handed spin along the head axis[34] (TABLE 2). Subsequent studies suggested that human sperm achieve control of spin handedness without a complex regulatory mechanism, but by asymmetric binding of molecular motors on the flagellum[206]. Human and horse sperm have been found to exhibit a 3D swimming pattern of chiral ribbons[45]. The planar swing of the sperm head occurs on an osculating plane, in some cases creating a helical ribbon and in others a twisted ribbon. Holographic imaging of >33,700 sperm trajectories revealed only 1.7% of human sperm exhibit chiral ribbons in comparison with 27.3% for horse sperm[45] (TABLE 2). These chiral ribbons might enable sperm to sense gradients of chemoattractants or temperature over large 3D volumes.

Microfluidics is a versatile tool for studying sperm behaviour and can be used to mimic the female reproductive tract geometrically and chemically[21]. Microchannels with complex geometries can be readily constructed using techniques such as soft lithography.

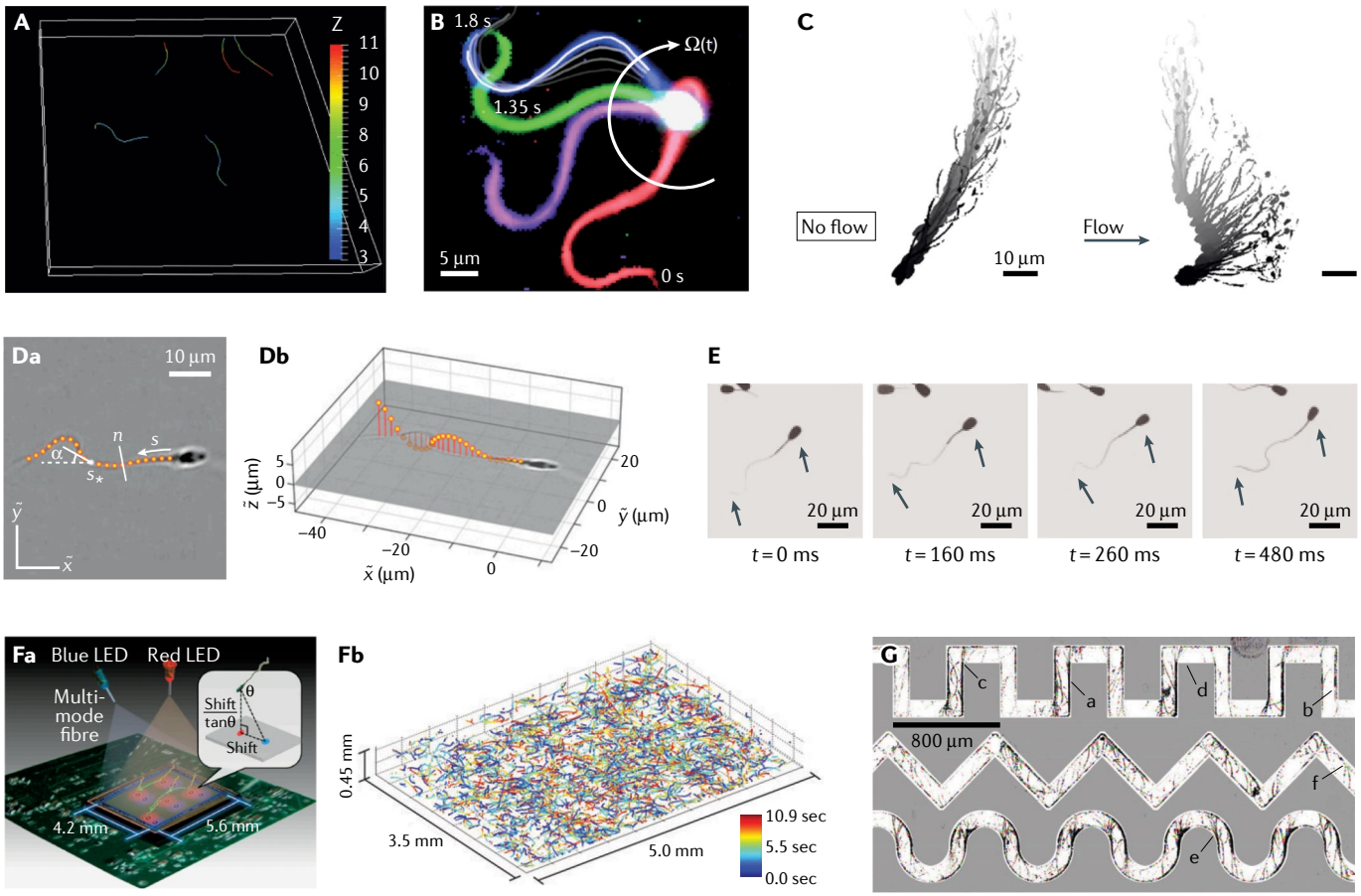

Fig. 4 | **Analysis of sperm locomotion and behaviour. A** | 3D contours of sperm flagella are extracted by a classifier to overcome low contrast. **B** | Four snapshots of a tethered human sperm that rotates clockwise around the tethering point. The flagellar beat pattern of human sperm displays a second-harmonic component. **C** | Sperm flagellum tracking showed no active asymmetry flagellum bending for control sperm under the no-flow condition and rheotaxis of sperm under flow. **D** | 2D image with tracked flagellum and 3D beat reconstruction to reveal that asymmetry of the midpiece determined the direction of rheotaxis turning. **E** | Total internal reflection fluorescence microscopy images showing a slithering swimming bovine sperm with the head confined within a few hundred nanometres of the substrate surface. **F** | Digital holography uses a sensor chip to record lens-free holograms on which basis the 3D trajectories of 1,575 human sperm inside a volume of 7.9 µl were reconstructed. **G** | Sperm exhibit boundary-following behaviour; most of the sperm swim along the intersection of the channel's vertical and horizontal walls, with few observed in the middle of the channel. LED, light-emitting diode. Part **A** is reprinted with permission from REF.[196], IEEE. Part **B** is reprinted from REF.[197], CC BY 4.0 (https://creativecommons.org/licenses/by/4.0/). Part **C** is reprinted from REF.[200], CC BY 4.0 (https://creativecommons.org/licenses/by/4.0/). Part **D** is reprinted with permission from REF.[201], PNAS. Part **E** is reprinted from REF.[46], CC BY 4.0 (https://creativecommons.org/licenses/by/4.0/). Part **F** is reprinted with permission from REF.[44], PNAS. Part **G** is reprinted with permission from REF.[47], PNAS.

Using microfluidic channels, sperm were shown to exhibit boundary-following behaviour[47]. Sperm were rarely observed to swim in the central part of the microchannel, instead travelling along the intersection of the channel walls (FIG. 4G; TABLE 2). Sperm left the channel wall when the curvature radius of the channel bend was less than ~150 μm[47]. Corner-swimming sperm were found to have a concentration as much as 200-fold that of the bulk-swimming sperm (TABLE 2). The relative degree of corner-swimming decreased with an increasing channel size and plateaued for channels above 200 μm[186]. The wall and corner swimming preferences of sperm were attributed to hydrodynamic interactions of sperm with surfaces. Time-averaged thrust was tilted towards the surface under the asymmetric hydrodynamic flow field near the surface[207]. This observation provides insight into sperm navigation within the female reproductive tract, especially the fallopian tube in the isthmus and ampulla with folded epithelium and narrow lumen and corner[186]. On-chip imaging by digital holography can be easily integrated into microchannel technology, enabling high-throughput analysis of sperm behaviour inside microchannels[208].

Discoveries concerning sperm locomotion and behaviour contribute to our understanding of sperm navigation inside the female reproductive tract, and the revealed behaviours can be used to design approaches for selecting sperm with high fertilization potential.

Subcellular and molecular structures

Conventional light microscopy does not have sufficient resolution to analyse the subcellular and molecular structure of sperm owing to its resolution of ~200 nm at the diffraction limit. Hence, super-resolution microscopy has been applied to investigate these features of sperm (FIG. 5). Scanning near-field optical microscopy (SNOM), which combines a scanning probe approach and optical microscopy, can achieve a spatial resolution of 50–100 nm[209]. In SNOM, the light is transmitted through a submicron aperture on a probe that causes a subwave length-sized spot to form, which is then scanned over a sperm to generate a super-resolution image. SNOM was used to analyse sperm mitochondria organization under the plasma membrane within the midpiece, revealing that mitochondria are helicoidally distributed around the axoneme[210] (FIG. 5A; TABLE 2). Few and disorganized mitochondria can cause severe asthenozoospermia (reduced sperm motility) or total immotility[63]. The organization and arrangement of circumferential ribs and longitudinal columns were also observed along the fibrous sheath of the sperm tail[210] (FIG. 5B). In patients with dysplasia of the fibrous sheath, the circumferential ribs and longitudinal columns are arranged without an orderly manner, leading to serious motility disorder and infertility[211].

Stochastic optical reconstruction microscopy (STORM) uses photoswitching to stochastically activate individual molecules at different times within the diffraction-limited region beyond the resolution of conventional microscopy[212]. Super-resolution images are then reconstructed from the measured positions of individual fluorophores. The resolution of STORM can reach 20 nm, but is limited by the accuracy of locating individual photoactivated fluorophores during a switching cycle[213]. Using STORM, CatSper channels were found to be normally distributed in linear quadrilateral domains along mouse sperm flagellum (FIG. 5C; TABLE 2), and Ca^{2+} signalling orchestrates tyrosine phosphorylation and motility[48]. Human CatSper is also quadrilaterally arranged along the flagellum[214] and is a progesterone receptor that induces Ca^{2+} influx[215]. STORM was also used to identify actin structures in mouse sperm tails; in the principal piece, actin is radially distributed between the axoneme and the plasma membrane. In the midpiece, actin forms a double-helix that accompanies mitochondria with a periodicity of 244 nm[216] (TABLE 2). This actin structure in the midpiece is involved in the compaction of mitochondria around the flagellum[217]. Whether this structure exists in human sperm requires further study.

Stimulated emission depletion (STED) microscopy is achieved by using the depletion laser to selectively deactivate fluorophores[218]. The depletion laser has a wavelength that is different from that of the excitation laser and is applied surrounding the focal spot of the excitation laser. In the region where both lasers overlap, the fluorophores are stimulated to emit photons with wavelength λ_{STED} rather than fluorescence photons with wavelength λ_F, decreasing the size of the region in which molecules fluoresce[218]. Scanning the focal spot across a sample enables a super-resolution image to be obtained with a resolution of ~20 nm. Using STED microscopy, a membrane cofactor protein, CD46, was shown to undergo dynamic reorganization over the mouse sperm head during the acrosome reaction[49] (FIG. 5D; TABLE 2). For sperm with an intact acrosome, CD46 was detected solely in the acrosomal cap, and after acrosome reaction CD46 filled the entire sperm head. CD46 was also found to have a role in stabilizing acrosomal membrane, and its relocation during acrosome reaction is driven by the actin cytoskeleton[49].

Structured illumination microscopy (SIM) uses the patterns of the excitation light to overcome the diffraction limit of conventional microscopy[219]. Typically, a sinusoidal pattern is created by combining two light beams; thus, a snapshot of the sample becomes the product of the sample's structure itself and the excitation pattern. A final image is then computationally reconstructed from multiple snapshots collected by scanning and rotating the pattern. The additional spatial modulation from the excitation pattern enhances the spatial resolution of the reconstructed image to ~100 nm[220]. Several custom-built SIM systems have been developed and demonstrated to be cost-effective[221,222]. Using SIM, membrane cofactor protein CD46 was found to be localized on the inner and outer acrosomal membrane of the mouse sperm head (FIG. 5E; TABLE 2), increasing understanding of its dynamic reorganization over the sperm head during acrosome reaction[49]. The use of SIM also helped to identify SUN4, a spermatid nuclear membrane protein that is essential for nuclear remodelling in spermiogenesis[223] (TABLE 2). SUN4 localizes to the pole of the nucleus distal to the acrosome and actin bundles in the mouse sperm head (FIG. 5F). The absence of the

protein in *SUN4*-knockout mice leads to the failure of nucleus elongation, and globozoospermia (round head) with associated infertility[223]. In human spermiogenesis, SUN4 was found to be necessary for maintaining the integrity of the nuclear envelope of sperm[224].

Immunostaining, which uses antibodies to detect specific proteins, has been used for identifying molecules in physiological processes such as capacitation and acrosome reaction. Abhydrolase domain-containing protein 2 (ABHD2) was found to be present on the human sperm tail (FIG. 5G) and it binds to progesterone[225]. In the presence of progesterone, ABHD2 activates CatSper channels by cleaving the CatSper inhibitor 2-arachidonoylglycerol (2AG). The activation of CatSper leads to a Ca^{2+} influx and the rise of intracellular Ca^{2+}, which initiates sperm hyperactivation and primes the sperm for the acrosome reaction[225] (TABLE 2). Immunostaining using antiphosphotyrosine antibodies showed that tyrosine phosphorylation is negatively regulated by Ca^{2+} influx and is part of the signal transduction pathway for capacitation[226]. Tyrosine phosphorylation was also shown to induce remodelling of the sperm plasma membrane to enable zona pellucida recognition[227]. Immunostaining also helped to identify sperm biomarkers that indicate infertility. For example, ubiquitin was found to be a biomarker of male infertility (FIG. 5H; TABLE 2). Abnormal sperm with head and tail defects and semen contaminants, such as spermatids and leukocytes, can be recognized by antiubiquitin antibodies[50]. The chaperone protein Heat Shock Protein Family A (Hsp70) Member 2 (HSPA2)

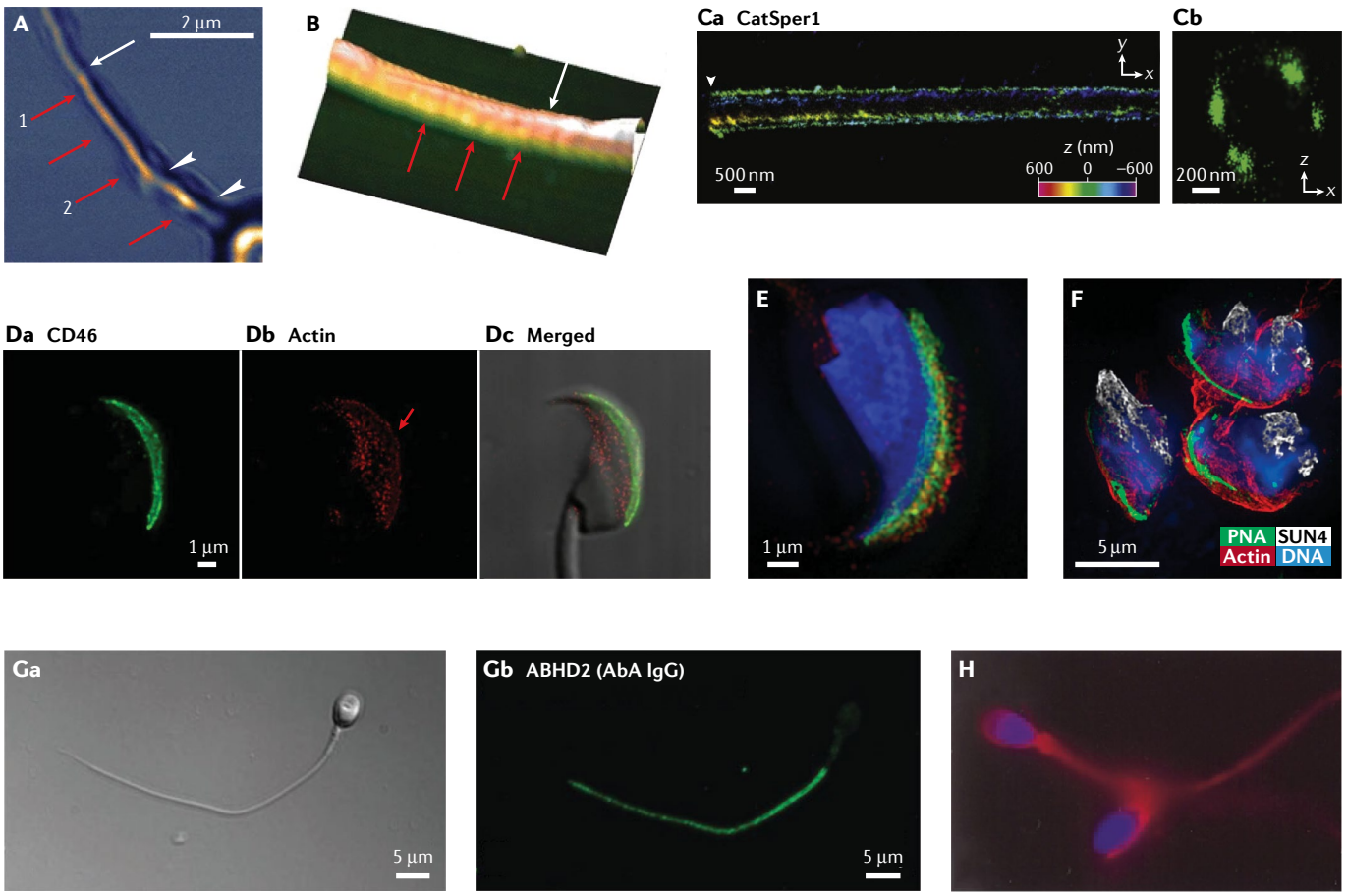

Fig. 5 | **Analysis of sperm structure and molecules. A** | Scanning near-field optical microscopy scan of the midpiece of a human sperm. White arrows indicate marked variations in optical contrast along the midpiece; red arrows indicate mitochondria. **B** | Scanning near-field optical microscopy topography of a sperm tail. Red arrows indicate the cross circumferential structures along the tail. **C** | 3D stochastic optical reconstruction microscopy images of CatSper1 in *x*–*y* and *y*–*z* cross-sections, indicating that CatSper proteins form four linear domains along mouse sperm flagellum. **D** | The distribution of CD46 and actin on the mouse sperm head imaged using stimulated emission depletion. CD46 exhibited a dynamic reorganization over the sperm head during the acrosome reaction. **E** | Stimulated emission depletion shows CD46 (green) localized on the inner and outer acrosomal membrane, and β1 integrin (red) localized on the outer acrosomal and plasma membrane of the acrosomal area of the mouse sperm. **F** | Structured illumination microscopy shows that SUN4, an essential protein for nuclear remodelling in spermiogenesis, is localized at the pole of the nucleus distal to the acrosome and actin bundles on mouse sperm head. **G** | Light microscopy of a human sperm and immunostaining of the same sperm with an anti-abhydrolase domain-containing protein 2 (ABHD2) antibody (AbA IgG). ABHD2 is distributed along the sperm tail and binds to progesterone to activate CatSper channels. **H** | Ubiquitin (red) profiles on sperm using immunostaining. Abnormal sperm with head and tail defects can be identified using anti-ubiquitin antibodies. AbA, antibodies against ABHD2; IgG, immunoglobulin; PNA, peanut agglutinin. Parts **A** and **B** are reprinted from REF.[210], CC BY 4.0 (https://creativecommons.org/licenses/by/4.0/). Part **C** is reprinted with permission from REF.[48], Elsevier. Parts **D** and **E** are reprinted from REF.[49], CC BY 4.0 (https://creativecommons.org/licenses/by/4.0/). Part **F** is adapted with permission from REF.[223], Elsevier. Part **G** is reprinted with permission from REF.[225], AAAS. Part **H** is adapted with permission from REF.[50], OUP.

was identified as a biomarker of human sperm maturation (TABLE 2), the expression level of which was positively correlated with sperm maturation, DNA integrity and chromatin maturity[52].Mass spectrometry is used to analyse molecules by ionizing and separating them using an electric or magnetic field based on the mass:charge ratio of the molecules[228]. Mass spectrometry was used to measure changes in protein phosphorylation during mouse sperm capacitation and enabled identification of 55 unique in vivo sites of phosphorylation and the extent of phosphorylation of 42 phosphopeptides[229] (TABLE 2). Protein phosphorylation forms the basis of intracellular signalling networks[230]. The discovered phosphorylation sites can help to reveal the signalling pathway for sperm capacitation. Mass spectrometry used to analyse human sperm revealed the presence of peptide residues potentially harbouring sites for post-translational modification. This observation suggests that protein modification is an important mechanism in sperm maturation[231]. This technology was also used to identify biomarkers for identifying azoospermia (no sperm in the semen)[232]. Epididymis-expressed extracellular matrix protein 1 (ECM1) was found to distinguish obstructive azoospermia from normal spermatogenesis with 100% specificity, and obstructive azoospermia from non-obstructive azoospermia with 73% specificity[232]. Testis-expressed protein 101 (TEX101) can further differentiate subtypes of non-obstructive azoospermia such as Sertoli cell-only syndrome[232] (TABLE 2). Profiling of oxysterol, an oxidized product of cholesterol, using mass spectrometry, enabled identification of 25-hydroxycholesterol expression as a biomarker of normal sperm[233]. Reduced levels of 25-hydroxycholesterol can negatively affect calcium and cholesterol movement into the acrosome region, causing ineffective acrosome reaction with the oocyte[233] (TABLE 2).

The discoveries made concerning sperm subcellular and molecular structures have been advanced by emerging techniques such as super-resolution microscopy and mass spectrometry. These discoveries provide insight into sperm physiology for processes such as capacitation and acrosome reaction, and help to identify biomarkers that are indicative of male infertility.

Future perspectives

Considerable advances have been made in sperm analysis; many current analysis techniques are invasive, defeating the purpose of selecting sperm for infertility treatment. Thus, efforts have been made to develop techniques for analysing sperm non-invasively. For example, automated measurement of live sperm morphology has been developed using advanced image processing, which enables real-time selection of morphologically normal sperm[35], to circumvent fixation and staining in traditional sperm morphology measurement. Techniques such as Raman spectroscopy have been attempted to non-invasively evaluate DNA fragmentation, but they require a specialized setup and specially trained staff, and might not fit into the workflow of typical clinical andrology settings. Alternatively, correlations between sperm morphology and DNA integrity have been established by non-invasively assessing sperm morphology with bright-field imaging[128] or interferometric phase microscopy[129] and quantitatively correlating DNA fragmentation with statistical[128] or machine learning models[130]. The established correlation can help to predict sperm DNA integrity without staining and also minimize disturbance to the standard clinical setup and workflow. Such prediction models are potentially valuable tools for selecting sperm with high DNA integrity for infertility treatment.

Sperm analysis can be used for prediction of ART outcomes, as sperm quality is an important determining factor. Via machine learning, sperm analysis results, along with other data such as maternal age and hormone levels, were used to train a model to predict implantation in IVF and ICSI[234]. Another model used logistic regression to predict the pregnancy in IVF based on sperm DNA fragmentation level[235]. The inclusion of discovered sperm biomarkers can help to further increase the prediction accuracy. These prediction models based on sperm analysis can improve male infertility assessment and management, and help to select the optimal ART procedures for patients.

Sperm analysis currently requires specific setup, personnel training and data analysis, which could benefit from automation and artificial intelligence techniques. Automation has the potential to increase efficiency by reducing manual involvement, improve accuracy by removing human error, and provide consistency in outcomes independent of operator training. Automated platforms have been developed for quantitative analysis of sperm concentration, motility and morphology[33,71]. Tedious sample preparation and sperm manipulation can be performed by robots, similar to robotic sample handling for DNA sequencing[236] and cancer diagnostics[237]. The promising deep-learning techniques[238] could enable the use of sperm images or videos to establish predictive models and select optimal sperm for use in ART[130]. The application of deep learning in sperm analysis[239] could help to identify subtle features or patterns that human observers are not able to identify, potentially improving infertility diagnosis and treatment.

Point-of-care sperm analysis is needed in remote and resource-limited areas. A portable lens-free microscopy imaging platform has been developed for visualizing sperm morphology using digital holography and pattern recognition[240]. Holographic shadows based on the shifts of the light source were captured and combined by image registration. The platform achieved a spatial resolution of 1.55 μm in a field of view of 30 mm^2. Smartphones have also been exploited for automated mobile diagnostics[241], with an attachment custom designed to contain lenses and an illuminator. The attachment's optical axis was aligned with the smartphone camera, and sperm images were captured by the camera and analysed via a smartphone application. It achieved sperm concentration and motility measurement with an accuracy of 98%[241]. Paper-based devices are low-cost diagnostic tools. The devices are fabricated by printing patterns of wax on paper and melting the wax to form hydrophobic barriers and chemical reagents are added into the patterned channels and reservoir of the device[242]. Sperm concentration and motility have been assessed with an

enzyme-based paper device, with the signals of enzyme reaction significantly different ($P < 0.01$) among samples with different sperm concentrations and motility[243]. Sperm DNA integrity measurement was also realized on a paper-based device by using Nafion to measure ion concentration polarization. The DNA fragmentation levels measured using this device strongly correlated ($R^2 > 0.86$) with those measured using SCSA[244]. The devices developed for point-of-care sperm analysis, owing to their low cost and ease of use, have the potential to offer affordable and easily accessible fertility diagnosis in resource-limited areas.

The discoveries enabled by sperm analysis have considerable translational value to clinical applications. For example, discoveries about sperm motion and guidance within the female reproductive tract can help to identify pathologies of male infertility, and observations of sperm behaviour can be used to select sperm for infertility treatment. Molecules found to be involved in sperm physiological processes, such as the acrosome reaction, can be used to develop enhancers or inhibitors for treatment or contraception purposes. The identified sperm biomarkers can be used to select mature and normal sperm for ART use. As more powerful techniques emerge, improved understanding of sperm behaviour, physiology and genetics will be gained, which in turn will lead to more effective, mechanism-targeted diagnostic and therapeutic approaches.

Integrating emerging techniques of sperm analysis into laboratories and clinics requires close collaboration between engineers, scientists and clinicians. During new technology development and testing, technique innovators must consider end-users' requirements, such as the constraints of time and cost, and scientists and clinicians must be consulted to provide guidance and perform quality assurance throughout the innovation process.

Conclusions

In the past decade, substantial advances in sperm analysis have been made, which have opened up new avenues for infertility diagnosis and treatment. Quantitative analysis of sperm motility, morphology and genetics provides valuable information for assessing male infertility and enables the selection of optimal sperm for ART. Emerging techniques improve accuracy, consistency and efficiency of the analysis, and enable new non-invasive measurement. Advances in sperm analysis also helped to reveal a multitude of discoveries in sperm locomotion and behaviour and subcellular and molecular structures. Distinct sperm behaviours, such as swimming along helical paths, have been shown, and molecules involved in physiological processes, such as capacitation and the acrosome reaction, have been discovered. Synergistic collaborations between multidisciplinary communities are essential for achieving improved sperm analysis, increasing discoveries regarding sperm behaviour and physiology, improving the success rates of infertility treatment, and increasing the benefits to patients and their children.

Published online: 01 June 2021

1. Vos, T. et al. Global, regional, and national incidence, prevalence, and years lived with disability for 310 diseases and injuries, 1990–2015: a systematic analysis for the Global Burden of Disease Study 2015. *Lancet* **388**, 1545–1602 (2016).
2. Agarwal, A. et al. A unique view on male infertility around the globe. *Reprod. Biol. Endocrinol.* **13**, 37 (2015).
3. Skakkebaek, N. E. et al. Male reproductive disorders and fertility trends: influences of environment and genetic susceptibility. *Physiol. Rev.* **96**, 55–97 (2016).
4. Vollset, S. E. et al. Fertility, mortality, migration, and population scenarios for 195 countries and territories from 2017 to 2100: a forecasting analysis for the Global Burden of Disease Study. *Lancet* **396**, 1285–1306 (2020).
5. Carlsen, E. et al. Evidence for decreasing quality of semen during past 50 years. *BMJ* **305**, 609–613 (1992).
6. Levine, H. et al. Temporal trends in sperm count: a systematic review and meta-regression analysis. *Hum. Reprod. Update* **23**, 646–659 (2017).
7. Sripada, S. et al. Trends in Semen Parameters in the Northeast of Scotland. *J. Androl.* **28**, 313–319 (2007).
8. Centola, G. M. et al. Decline in sperm count and motility in young adult men from 2003 to 2013: observations from a U . S . sperm bank. *Andrology* **4**, 270–276 (2016).
9. Virtanen, H. E. & Toppari, J. Semen quality in the 21 st century. *Nat. Rev. Urol.* **14**, 120–130 (2017).
10. World Health Organization. *WHO Laboratory Manual for the Examination and Processing of Human Semen*. https://www.who.int/docs/default-source/reproductive-health/srhr-documents/infertility/examination-and-processing-of-human-semen-5ed-eng.pdf?sfvrsn=5227886e_2 (2010).
11. David, S. et al. Sperm morphology, motility, and concentration in fertile and infertile men. *N. Engl. J. Med.* **345**, 1388–1393 (2001).
12. Donnelly, E. T. et al. In vitro fertilization and pregnancy rates: the influence of sperm motility and morphology on IVF outcome. *Fertil. Steril.* **70**, 305–314 (1998).
13. Bartoov, B. et al. Real-time fine morphology of motile human sperm cells is associated with IVF-ICSI outcome. *J. Androl.* **23**, 1–8 (2002).
14. De Vos, A. et al. Influence of individual sperm morphology on fertilization, embryo morphology, and pregnancy outcome of intracytoplasmic sperm injection. *Fertil. Steril.* **79**, 42–48 (2003).
15. Evenson, D. P. The Sperm Chromatin Structure Assay (SCSA) and other sperm DNA fragmentation tests for evaluation of sperm nuclear DNA integrity as related to fertility. *Anim. Reprod. Sci.* **169**, 56–75 (2016).
16. Ramasamy, R., Besada, S. & Lamb, D. J. Fluorescent in situ hybridization of human sperm: Diagnostics, indications, and therapeutic implications. *Fertil. Steril.* **102**, 1534–1539 (2014).
17. Zini, A., San Gabriel, M. & Baazeem, A. Antioxidants and sperm DNA damage: a clinical perspective. *J. Assist. Reprod. Genet.* **26**, 427–432 (2009).
18. Baldi, E., & Muratori, M. *Genetic Damage in Human Spermatozoa* (Springer, 2014).
19. Zidi-Jrah, I. et al. Relationship between sperm aneuploidy, sperm DNA integrity, chromatin packaging, traditional semen parameters, and recurrent pregnancy loss. *Fertil. Steril.* **105**, 58–64 (2016).
20. Esteves, S. C., Roque, M., Bradley, C. K. & Garrido, N. Reproductive outcomes of testicular versus ejaculated sperm for intracytoplasmic sperm injection among men with high levels of DNA fragmentation in semen: systematic review and meta-analysis. *Fertil. Steril.* **108**, 456–467 (2017).
21. Nosrati, R. et al. Microfluidics for sperm analysis and selection. *Nat. Rev. Urol.* **14**, 707 (2017).
22. Esteves, S. C., Roque, M., Bedoschi, G., Haahr, T. & Humaidan, P. Intracytoplasmic sperm injection for male infertility and consequences for offspring. *Nat. Rev. Urol.* **15**, 1–28 (2018).
23. Adamson, G. D. et al. International committee for monitoring assisted reproductive technology: world report on assisted reproductive technology, 2011. *Fertil. Steril.* **110**, 1067–1080 (2018).
24. Sunderam, S. et al. Assisted reproductive technology surveillance — United States, 2012. *Morbidity Mortal. Wkly. Report Surveill. Summaries* **64**, 1–29 (2015).
25. Wyns, C. et al. ART in Europe, 2016: results generated from European registries by ESHRE. *Hum. Reprod. Open* **3**, hoaa032 (2020).
26. Gnoth, C. et al. Final ART success rates: a 10 years survey. *Hum. Reprod.* **26**, 2239–2246 (2011).
27. Em, S. et al. The impact of sperm DNA damage in assisted conception and beyond: recent advances in diagnosis and treatment. *Reprod. Biomed. Online* **27**, 325–337 (2013).
28. Eamer, L. et al. Turning the corner in fertility: high DNA integrity of boundary-following sperm. *Lab. Chip* **16**, 2418–2422 (2016).
29. Parmegiani, L. et al. "Physiologic ICSI": Hyaluronic acid (HA) favors selection of spermatozoa without DNA fragmentation and with normal nucleus, resulting in improvement of embryo quality. *Fertil. Steril.* **93**, 598–604 (2010).
30. Hoogendijk, C. F., Ph, D., Kruger, T. F., Bouic, P. J. D. & Ph, D. A novel approach for the selection of human sperm using annexin V-binding and flow cytometry. *Fertil. Steril.* **91**, 1285–1292 (2009).
31. Miller, D. et al. Physiological, hyaluronan-selected intracytoplasmic sperm injection for infertility treatment (HABSelect): a parallel, two-group, randomised trial. *Lancet* **393**, 416–422 (2019).
32. Sakkas, D., Ramalingam, M., Garrido, N. & Barratt, C. L. Sperm selection in natural conception: what can we learn from Mother Nature to improve assisted reproduction outcomes? *Hum. Reprod. Update* **21**, 711–726 (2015).
33. Amann, R. P. & Katz, D. F. Andrology lab corner: reflections on CASA after 25 years. *J. Androl.* **25**, 317–325 (2004).
34. Daloglu, M. U. et al. Label-free 3D computational imaging of spermatozoon locomotion, head spin and flagellum beating over a large volume. *Light. Sci. Appl.* **7**, 17111–17121 (2018).
35. Dai, C. et al. Automated non-invasive measurement of single sperm's motility and morphology. *IEEE Trans. Med. Imaging* **37**, 2257–2265 (2018).

36. Sánchez, V. et al. Oxidative DNA damage in human sperm can be detected by Raman microspectroscopy. *Fertil. Steril.* **98**, 1124–1129 (2012).
37. Nazarenko, R. V., Irzhak, A. V., Pomerantsev, A. L. & Rodionova, O. Y. Confocal Raman spectroscopy and multivariate data analysis for evaluation of spermatozoa with normal and abnormal morphology. A feasibility study. *Chemom. Intell. Lab. Syst.* **182**, 172–179 (2018).
38. Sequencing, W. et al. Probing meiotic recombination and aneuploidy of single sperm cells by whole-genome sequencing. *Science* **338**, 1627–1631 (2012).
39. Tran, Q. T. et al. Chromosomal scan of single sperm cells by combining fluorescence-activated cell sorting and next-generation sequencing. *J. Assist. Reprod. Genet.* **36**, 91–97 (2019).
40. Nosrati, R. et al. Rapid selection of sperm with high DNA integrity. *Lab. Chip* **14**, 1142 (2014).
41. Wagenaar, B. D., Dekker, S., Olthuis, W., Berg, A. V. D. & Segerink, L. I. Towards microfluidic sperm refinement: continuous flow label-free analysis and sorting of sperm cells. *Lab. Chip* **16**, 528–530 (2015).
42. Zaferani, M., Cheong, S. H. & Abbaspourrad, A. Rheotaxis-based separation of sperm with progressive motility using a microfluidic corral system. *Proc. Natl Acad. Sci. USA* **115**, 8272–8277 (2018).
43. Bucar, S. et al. DNA fragmentation in human sperm after magnetic-activated cell sorting. *J. Assist. Reprod. Genet.* **32**, 147–154 (2015).
44. Su, T.-W., Xue, L. & Ozcan, A. High-throughput lensfree 3D tracking of human sperms reveals rare statistics of helical trajectories. *Proc. Natl Acad. Sci. USA* **109**, 16018–16022 (2012).
45. Su, T. W. et al. Sperm trajectories form chiral ribbons. *Sci. Rep.* **3**, 1–8 (2013).
46. Nosrati, R., Driouchi, A., Yip, C. M. & Sinton, D. Two-dimensional slither swimming of sperm within a micrometre of a surface. *Nat. Commun.* **6**, 8703 (2015).
47. Denissenko, P., Kantsler, V., Smith, D. J. & Kirkman-Brown, J. Human spermatozoa migration in microchannels reveals boundary-following navigation. *Proc. Natl Acad. Sci. USA* **109**, 8007–8010 (2012).
48. Chung, J. J. et al. Structurally distinct Ca^{2+} signaling domains of sperm flagella orchestrate tyrosine phosphorylation and motility. *Cell* **157**, 808–822 (2014).
49. Frolikova, M., Sebkova, N., Ded, L. & Dvorakova-Hortova, K. Characterization of CD46 and β1 integrin dynamics during sperm acrosome reaction. *Sci. Rep.* **6**, 1–15 (2016).
50. Sutovsky, P., Terada, Y. & Schatten, G. Ubiquitin-based sperm assay for the diagnosis of male factor infertility. *Hum. Reprod.* **16**, 250–258 (2001).
51. Schiza, C. G., Jarvi, K., Diamandis, E. P. & Drabovich, A. P. An emerging role of TEX101 protein as a male infertility biomarker. *J. Int. Fed. Clin. Chem. Lab. Med.* **25**, 9–26 (2014).
52. Huszar, G. Biochemical markers of sperm function: male fertility and sperm selection for ICSI. *Reprod. Biomed. Online* **7**, 462–468 (2003).
53. Louis, G. M. B. et al. Semen quality and time to pregnancy: the longitudinal investigation of fertility and the environment study. *Fertil. Steril.* **101**, 453–462 (2014).
54. Zinaman, M. J., Brown, C. C., Selevan, S. G. & Clegg, E. D. Semen quality and human fertility: a prospective study with healthy couples. *J. Androl.* **21**, 145–153 (2000).
55. Bonde, J. P. E. et al. Relation between semen quality and fertility: a population-based study of 430 first-pregnancy planners. *Lancet* **352**, 1172–1177 (1998).
56. Bungum, M. et al. Sperm DNA integrity assessment in prediction of assisted reproduction technology outcome. *Hum. Reprod.* **22**, 174–179 (2007).
57. Duran, E. H., Morshedi, M., Taylor, S. & Oehninger, S. Sperm DNA quality predicts intrauterine insemination outcome: a prospective cohort study. *Hum. Reprod.* **17**, 3122–3128 (2002).
58. Marques, C. J. et al. Abnormal methylation of imprinted genes in human sperm is associated with oligozoospermia. *Mol. Hum. Reprod.* **14**, 67–73 (2008).
59. Jenkins, T. G. et al. Sperm epigenetics in the study of male fertility, offspring health, and potential clinical applications. *Syst. Biol. Reprod. Med.* **63**, 69–76 (2017).
60. Turner, R. M. Moving to the beat: a review of mammalian sperm motility regulation. *Reprod. Fertil. Dev.* **18**, 25–38 (2005).
61. Gaffney, E. et al. Mammalian sperm motility: observation and theory. *Annu. Rev. Fluid Mech.* **43**, 501–528 (2011).
62. Lindemann, C. B. & Lesich, K. A. Functional anatomy of the mammalian sperm flagellum. *Cytoskeleton* **73**, 652–669 (2016).
63. Piomboni, P., Focarelli, R., Stendardi, A., Ferramosca, A. & Zara, V. The role of mitochondria in energy production for human sperm motility. *Int. J. Androl.* **35**, 109–124 (2012).
64. Vernon, G. G. & Woolley, D. M. Basal sliding and the mechanics of oscillation in a mammalian sperm flagellum. *Biophys. J.* **87**, 3934–3944 (2004).
65. Guzick, D. S. et al. Sperm morphology, motility, and concentration in fertile and infertile men. *N. Engl. J. Med.* **345**, 1388–1393 (2001).
66. Lu, J. C., Huang, Y. F. & Lu, N. Q. Computer-aided sperm analysis: past, present and future. *Andrologia* **46**, 329–338 (2014).
67. Amann, R. P. & Waberski, D. Computer-assisted sperm analysis (CASA): capabilities and potential developments. *Theriogenology* **81**, 5–17 (2014).
68. Chenouard, N. et al. Objective comparison of particle tracking methods. *Nat. Methods* **11**, 281–289 (2014).
69. Urbano, L., Masson, P., VerMilyea, M. & Kam, M. Automatic tracking and motility analysis of human sperm in time-lapse images. *IEEE Trans. Med. Imaging* **36**, 792–801 (2016).
70. Tomlinson, M. J. et al. Validation of a novel computer-assisted sperm analysis (CASA) system using multitarget-tracking algorithms. *Fertil. Steril.* **93**, 1911–1920 (2010).
71. Agarwal, A., Henkel, R., Huang, C. C. & Lee, M. S. Automation of human semen analysis using a novel artificial intelligence optical microscopic technology. *Andrologia* **51**, 13440 (2019).
72. Menkveld, R. et al. Semen parameters, including WHO and strict criteria morphology, in a fertile and subfertile population: an effort towards standardization of in-vivo thresholds. *Hum. Reprod.* **16**, 1165–1171 (2001).
73. Bijar, A., Benavent, A. P., Mikaeili, M. & Khayati, R. Fully automatic identification and discrimination of sperm's parts in microscopic images of stained human semen smear. *J. Biomed. Sci. Eng.* **5**, 384–395 (2012).
74. Maree, L., Du Plessis, S. S., Menkveld, R. & Van der Horst, G. Morphometric dimensions of the human sperm head depend on the staining method used. *Hum. Reprod.* **25**, 1369–1382 (2010).
75. Perdrix, A. & Rives, N. Motile sperm organelle morphology examination (MSOME) and sperm head vacuoles: state of the art in 2013. *Hum. Reprod. Update* **19**, 527–541 (2013).
76. Berkovitz, A. et al. The morphological normalcy of the sperm nucleus and pregnancy rate of intracytoplasmic injection with morphologically selected sperm. *Hum. Reprod.* **20**, 185–190 (2005).
77. Setti, A. S., Braga, D. P., Iaconelli, A., Aoki, T. & Borges, E. Twelve years of MSOME and IMSI: a review. *Reprod. Biomed. Online* **27**, 338–352 (2013).
78. Hammoud, I. et al. Selection of normal spermatozoa with a vacuole-free head (×6300) improves selection of spermatozoa with intact DNA in patients with high sperm DNA fragmentation rates. *Andrologia* **45**, 163–170 (2013).
79. Balaban, B. et al. Clinical outcome of intracytoplasmic injection of spermatozoa morphologically selected under high magnification: a prospective randomized study. *Reprod. Biomed. Online* **22**, 472–476 (2011).
80. De Vos, A. et al. Does intracytoplasmic morphologically selected sperm injection improve embryo development? A randomized sibling-oocyte study. *Hum. Reprod.* **28**, 617–626 (2013).
81. Ebner, T., Shebl, O., Oppelt, P. & Mayer, R. B. Some reflections on intracytoplasmic morphologically selected sperm injection. *Int. J. Fertil. Steril.* **8**, 105 (2014).
82. Rougier, N. et al. Changes in DNA fragmentation during sperm preparation for intracytoplasmic sperm injection over time. *Fertil. Steril.* **100**, 69–74 (2013).
83. Vingris, L. et al. Sperm morphological normality under high magnification predicts laboratory and clinical outcomes in couples undergoing ICSI. *Hum. Fertil.* **18**, 81–86 (2015).
84. Dai, C. et al. Automated motility and morphology measurement of live spermatozoa. *Andrology* https://doi.org/10.1111/andr.13002 (2021).
85. Yin, Z., Kanade, T. & Chen, M. Understanding the phase contrast optics to restore artifact-free microscopy images for segmentation. *Med. Image Anal.* **16**, 1047–1062 (2012).
86. Obara, B., Roberts, M. A., Armitage, J. P. & Grau, V. Bacterial cell identification in differential interference contrast microscopy images. *BMC Bioinform.* **14**, 1–3 (2013).
87. Shaked, N. T. Label-free quantitative imaging of sperm for in-vitro fertilization using interferometric phase microscopy. *JFIV Reprod. Med. Genet.* **4**, 190 (2016).
88. Coppola, G. et al. Digital holographic microscopy for the evaluation of human sperm structure. *Zygote* **22**, 446–454 (2014).
89. Haifler, M. et al. Interferometric phase microscopy for label-free morphological evaluation of sperm cells. *Fertil. Steril.* **104**, 43–47 (2015).
90. Almeling, R. Selling genes, selling gender: Egg agencies, sperm banks, and the medical market in genetic material. *Am. Sociol. Rev.* **72**, 319–340 (2007).
91. Bisht, S., Faiq, M., Tolahunase, M. & Dada, R. Oxidative stress and male infertility. *Nat. Rev. Urol.* **14**, 470–85 (2017).
92. Tang, S. et al. Biallelic mutations in CFAP43 and CFAP44 cause male infertility with multiple morphological abnormalities of the sperm flagella. *Am. J. Hum. Genet.* **100**, 854–864 (2017).
93. Firat-karalar, E. N., Sante, J., Elliott, S. & Stearns, T. Proteomic analysis of mammalian sperm cells identifies new components of the centrosome. *J. Cell Sci.* **3**, 4128–4133 (2014).
94. Coutton, C. et al. Bi-allelic mutations in ARMC2 lead to severe astheno-teratozoospermia due to sperm flagellum malformations in humans and mice. *Am. J. Hum. Genet.* **104**, 331–340 (2019).
95. Zhu, F. et al. Biallelic SUN5 mutations cause autosomal-recessive acephalic spermatozoa syndrome. *Am. J. Hum. Genet.* **99**, 942–949 (2016).
96. Zhu, F. et al. Mutations in PMFBP1 cause acephalic spermatozoa syndrome. *Am. J. Hum. Genet.* **103**, 188–199 (2018).
97. Krausz, C. & Riera-Escamilla, A. Genetics of male infertility. *Nat. Rev. Urol.* **15**, 1–16 (2018).
98. Lewis, S. E. & Simon, L. Clinical implications of sperm DNA damage. *Hum. Fertil.* **13**, 201–207 (2010).
99. Evenson, D. P. Evaluation of sperm chromatin structure and DNA strand breaks is an important part of clinical male fertility assessment. *Transl. Androl. Urol.* **6**, 2–7 (2017).
100. Evenson, D. & Wixon, R. Meta-analysis of sperm DNA fragmentation using the sperm chromatin structure assay. *Reprod. Biomed. Online* **12**, 466–472 (2006).
101. Shamsi, M. B., Imam, S. N. & Dada, R. Sperm DNA integrity assays: Diagnostic and prognostic challenges and implications in management of infertility. *J. Assist. Reprod. Genet.* **28**, 1073–1085 (2011).
102. Mishra, S., Kumar, R., Malhotra, N., Singh, N. & Dada, R. Mild oxidative stress is beneficial for sperm telomere length maintenance. *World J. Methodol.* **6**, 163 (2016).
103. Tremellen, K. Oxidative stress and male infertility — a clinical perspective. *Hum. Reprod. Update* **14**, 243–258 (2008).
104. Lewis, S. E. & Aitken, R. J. DNA damage to spermatozoa has impacts on fertilization and pregnancy. *Cell Tissue Res.* **322**, 33–41 (2005).
105. Kumar, S. B., Chawla, B., Bisht, S., Yadav, R. K. & Dada, R. Tobacco use increases oxidative DNA damage in sperm-possible etiology of childhood cancer. *Asian Pac. J. Cancer Prev.* **16**, 6967–6972 (2015).
106. Vorilhon, S. et al. Accuracy of human sperm DNA oxidation quantification and threshold determination using an 8-OHdG immuno-detection assay. *Hum. Reprod.* **33**, 553–562 (2018).
107. Muratori, M. et al. Investigation on the origin of sperm DNA fragmentation: role of apoptosis, immaturity and oxidative stress. *Mol. Med.* **21**, 109–122 (2015).
108. Ni, K., Spiess, A. N., Schuppe, H. C. & Steger, K. The impact of sperm protamine deficiency and sperm DNA damage on human male fertility: a systematic review and meta-analysis. *Andrology* **4**, 789–799 (2006).
109. Sakkas, D., Seli, E., Bizzaro, D., Tarozzi, N. & Manicardi, G. C. Abnormal spermatozoa in the ejaculate: abortive apoptosis and faulty nuclear remodelling during spermatogenesis. *Reprod. Biomed. Online* **7**, 428–432 (2003).
110. Virro, M. R., Larson-cook, K. L. & Evenson, D. P. Sperm chromatin structure assay (SCSA) parameters are related to fertilization, blastocyst development, and ongoing pregnancy in in vitro fertilization and intracytoplasmic sperm injection cycles. *Fertil. Steril.* **81**, 1289–1295 (2004).
111. Henkel, R., Hoogendijk, C. F., Bouic, P. J. D. & Kruger, T. F. TUNEL assay and SCSA determine different aspects of sperm DNA damage. *Andrologia* **42**, 305–313 (2010).
112. Sergerie, M., Laforest, G., Bujan, L., Bissonnette, F. & Bleau, G. Sperm DNA fragmentation: threshold value in male fertility. *Hum. Reprod.* **20**, 3446–3451 (2005).

113. Ribeiro, S. et al. Inter- and intra-laboratory standardization of TUNEL assay for assessment of sperm DNA fragmentation. *Andrology* **5**, 477–485 (2017).
114. Mitchell, L. A., Iuliis, G. N. D. & Aitken, R. J. The TUNEL assay consistently underestimates DNA damage in human spermatozoa and is influenced by DNA compaction and cell vitality: development of an improved methodology. *Int. J. Androl.* **34**, 2–13 (2010).
115. Muratori, M., Forti, G. & Baldi, E. Comparing flow cytometry and fluorescence microscopy for analyzing human sperm DNA fragmentation by TUNEL labeling. *Cytom. A* **73**, 785–787 (2008).
116. Cho, C. L. & Agarwal, A. Role of sperm DNA fragmentation in male factor infertility: a systematic review. *Arab. J. Urol.* **16**, 21–34 (2018).
117. Muriel, L. et al. The sperm chromatin dispersion test: a simple method for the determination of sperm DNA fragmentation. *J. Androl.* **24**, 59–66 (2003).
118. Morris, I. D., Ilott, S., Dixon, L. & Brison, D. R. The spectrum of DNA damage in human sperm assessed by single cell gel electrophoresis (Comet assay) and its relationship to fertilization and embryo development. *Hum. Reprod.* **17**, 990–998 (2002).
119. Afanasieva, K. & Sivolob, A. Biophysical chemistry physical principles and new applications of comet assay. *Biophys. Chem.* **238**, 1–7 (2018).
120. Collins, A. R. et al. The comet assay: topical issues. *Mutagenesis* **23**, 143–151 (2008).
121. Olive, P. L. & Banáth, J. P. The comet assay: a method to measure DNA damage in individual cells. *Nat. Protoc.* **1**, 23 (2006).
122. Simon, L. et al. Sperm DNA damage measured by the alkaline Comet assay as an independent predictor of male infertility and in vitro fertilization success. *Fertil. Steril.* **95**, 652–657 (2011).
123. Ribas-Maynou, J. et al. Double stranded sperm DNA breaks measured by comet assay, are associated with unexplained recurrent miscarriage in couples without a female factor. *PLoS ONE* **7**, 44679 (2012).
124. Sanchez, V. et al. Oxidative DNA damage in human sperm can be detected by Raman microspectroscopy. *Fertil. Steril.* **98**, 1124–9 (2012).
125. Angelis, A. De et al. Combined Raman spectroscopy and digital holographic microscopy for sperm cell quality analysis. *J. Spectrosc.* **2017**, 1–15 (2017).
126. Boydston-white, S., Mattha, C., Romeo, M. & Diem, M. A. X. Raman and infrared microspectral imaging of mitotic cells. *Appl. Spectrosc.* **60**, 1–8 (2006).
127. Costa, R. Da, Amaral, S., Redmann, K., Kliesch, S. & Id, S. S. Spectral features of nuclear DNA in human sperm assessed by raman microspectroscopy: effects of UV-irradiation and hydration. *PLoS ONE* **13**, 1–15 (2018).
128. Wang, Y. et al. Prediction of DNA integrity from morphological parameters using a single-sperm DNA fragmentation index assay. *Adv. Sci.* **6**, 1900712 (2019).
129. Barnea, I. et al. Stain-free interferometric phase microscopy correlation with DNA fragmentation stain in human spermatozoa. *J. Biophotonics* **11**, 1–10 (2018).
130. McCallum, C. et al. Deep learning-based selection of human sperm with high DNA integrity. *Commun. Biol.* **2**, 1–100 (2019).
131. Calogero, A. E. et al. Sperm aneuploidy in infertile men. *Reprod. Biomed. Online* **6**, 310–317 (2003).
132. Shi, Q. & Martin, R. H. Aneuploidy in human sperm: a review of the frequency and distribution of aneuploidy, effects of donor age and lifestyle factors. *Cytogenet. Cell Genet.* **90**, 219–226 (2000).
133. Hassold, T. & Hunt, P. To err (meiotically) is human: the genesis of human aneuploidy. *Nat. Rev. Genet.* **2**, 280–291 (2001).
134. Muriel, L. et al. Increased aneuploidy rate in sperm with fragmented DNA as determined by the sperm chromatin dispersion (SCD) test and FISH analysis. *J. Androl.* **28**, 38–49 (2007).
135. Huber, D., Voithenberg, L. V. V. & Kaigala, G. V. Fluorescence in situ hybridization (FISH): History, limitations and what to expect from micro-scale FISH? *Micro Nano Eng.* **1**, 15–24 (2018).
136. Song, S. H. et al. Genome-wide screening of severe male factor infertile patients using BAC-array comparative genomic hybridization (CGH). *Gene* **506**, 248–252 (2012).
137. Karampetsou, E., Morrogh, D. & Chitty, L. Microarray technology for the diagnosis of fetal chromosomal aberrations: which platform should we use? *J. Clin. Med.* **3**, 663–678 (2014).
138. Rubio, C. et al. Use of array comparative genomic hybridization (array-CGH) for embryo assessment: clinical results. *Fertil. Steril.* **99**, 1044–1048 (2013).
139. Patassini, C. et al. Molecular karyotyping of human single sperm by array- comparative genomic hybridization. *PLoS ONE* **8**, 60922 (2013).
140. Xi, R., Kim, T. & Park, P. J. Detecting structural variations in the human genome using next generation sequencing. *Brief. Funct. Genomics* **9**, 405–415 (2011).
141. Koboldt, D. C., Steinberg, K. M., Larson, D. E., Wilson, R. K. & Mardis, E. R. The next-generation sequencing revolution and its impact on genomics. *Cell* **155**, 27–38 (2013).
142. Cheung, S., Parrella, A., Rosenwaks, Z. & Palermo, G. D. Genetic and epigenetic profiling of the infertile male. *PLoS ONE* **14**, e0214275 (2019).
143. Kazda, A. et al. Chromosome end protection by blunt-ended telomeres. *Genes Dev.* **26**, 1703–1713 (2012).
144. Nandakumar, J. & Cech, T. R. Finding the end: recruitment of telomerase to telomeres. *Nat. Rev. Mol. Cell Biol.* **14**, 69–82 (2013).
145. Thilagavathi, J. et al. Analysis of sperm telomere length in men with idiopathic infertility. *Arch. Gynecol. Obstet.* **287**, 803–807 (2013).
146. Yang, Q. et al. Sperm telomere length is positively associated with the quality of early embryonic development. *Hum. Reprod.* **30**, 1876–1881 (2015).
147. Boniewska-Bernacka, E., Pańczyszyn, A. & Cybulska, N. Telomeres as a molecular marker of male infertility. *Hum. Fertil.* **22**, 78–87 (2019).
148. Lafuente, R. et al. Sperm telomere length in motile sperm selection techniques: a qFISH approach. *Andrologia* **50**, e12840 (2018).
149. Turner, S. & Hartshorne, G. M. Telomere lengths in human pronuclei, oocytes and spermatozoa. *Mol. Hum. Reprod.* **19**, 510–518 (2013).
150. Cariati, F. et al. Investigation of sperm telomere length as a potential marker of paternal genome integrity and semen quality. *Reprod. Biomed. Online* **33**, 404–411 (2016).
151. Zhao, F., Yang, Q., Shi, S., Luo, X. & Sun, Y. Semen preparation methods and sperm telomere length: density gradient centrifugation versus the swim up procedure. *Sci. Rep.* **6**, 39051 (2016).
152. Rocca, M. S., Foresta, C. & Ferlin, A. Telomere length: lights and shadows on their role in human reproduction. *Biol. Reprod.* **100**, 305–317 (2019).
153. Jenkins, T. G. & Carrell, D. T. The sperm epigenome and potential implications for the developing embryo. *Reproduction* **143**, 727 (2012).
154. Hammoud, S. S. et al. Genome-wide analysis identifies changes in histone retention and epigenetic modifications at developmental and imprinted gene loci in the sperm of infertile men. *Hum. Reprod.* **26**, 2558–2569 (2011).
155. Denomme, M. M., McCallie, B. R., Parks, J. C., Schoolcraft, W. B. & Katz-Jaffe, M. G. Alterations in the sperm histone-retained epigenome are associated with unexplained male factor infertility and poor blastocyst development in donor oocyte IVF cycles. *Hum. Reprod.* **32**, 2443–2455 (2017).
156. Aston, K. I. et al. Aberrant sperm DNA methylation predicts male fertility status and embryo quality. *Fertil. Steril.* **104**, 1388–1397 (2015).
157. Schrott, R. et al. Sperm DNA methylation altered by tHc and nicotine: vulnerability of neurodevelopmental genes with bivalent chromatin. *Sci. Rep.* **10**, 1–12 (2020).
158. Maamar, M. B. et al. Developmental origins of transgenerational sperm DNA methylation epimutations following ancestral DDT exposure. *Dev. Biol.* **445**, 280–293 (2019).
159. Jenkins, T. G. et al. Intra-sample heterogeneity of sperm DNA methylation. *Mol. Hum. Reprod.* **21**, 313–319 (2015).
160. Keravnou, A. et al. Whole-genome fetal and maternal DNA methylation analysis using MeDIP-NGS for the identification of differentially methylated regions. *Genet. Res.* **98**, 1–9 (2016).
161. Luján, S. et al. Sperm DNA methylation epimutation biomarkers for male infertility and FSH therapeutic responsiveness. *Sci. Rep.* **9**, 1–12 (2019).
162. Oostlander, A. E., Meijer, G. A. & Ylstra, B. Microarray-based comparative genomic hybridization and its applications in human genetics. *Clin. Genet.* **66**, 488–495 (2004).
163. Houshdaran, S. et al. Widespread epigenetic abnormalities suggest a broad DNA methylation erasure defect in abnormal human sperm. *PLoS ONE* **2**, e1289 (2007).
164. Aston, K. I. et al. Genome-wide sperm deoxyribonucleic acid methylation is altered in some men with abnormal chromatin packaging or poor in vitro fertilization embryogenesis. *Fertil. Steril.* **97**, 285–292 (2012).
165. Brykczynska, U. et al. Repressive and active histone methylation mark distinct promoters in human and mouse spermatozoa. *Nat. Struct. Mol. Biol.* **17**, 679 (2010).
166. Steilmann, C. et al. Presence of histone H3 acetylated at lysine 9 in male germ cells and its distribution pattern in the genome of human spermatozoa. *Reprod. Fertil. Dev.* **23**, 997–1011 (2011).
167. Hammoud, S. S. et al. Distinctive chromatin in human sperm packages genes for embryo development. *Nature* **460**, 473–478 (2009).
168. Boissonnas, C., Ph, D. & Jouannet, P. Epigenetic disorders and male subfertility. *Fertil. Steril.* **99**, 624–631 (2013).
169. Hamatani, T. Human spermatozoal RNAs. *Fertil. Steril.* **97**, 275–281 (2012).
170. Pelloni, M. et al. Molecular study of human sperm RNA: ropporin and CABYR in asthenozoospermia. *J. Endocrinol. Invest.* **41**, 781–787 (2018).
171. Gòdia, M. et al. A RNA-Seq analysis to describe the boar sperm transcriptome and its seasonal changes. *Front. Genet.* **10,**, 299 (2019).
172. Wein, S. et al. A computational platform for high-throughput analysis of RNA sequences and modifications by mass spectrometry. *Nat. Commun.* **11**, 1–12 (2020).
173. Kukurba, K. R. & Montgomery, S. B. RNA sequencing and analysis. *Cold Spring Harb. Protoc.* **2015**, 951–969 (2015).
174. Aoki, V. W., Liu, L. & Carrell, D. T. A novel mechanism of protamine expression deregulation highlighted by abnormal protamine transcript retention in infertile human males with sperm protamine deficiency. *Mol. Hum. Reprod.* **12**, 41–50 (2006).
175. Ostermeier, G. C., Miller, D., Huntriss, J. D., Diamond, M. P. & Krawetz, S. A. Delivering spermatozoan RNA to the oocyte. *Nature* **429**, 154 (2004).
176. Rassoulzadegan, M. et al. RNA-mediated non-mendelian inheritance of an epigenetic change in the mouse. *Nature* **441**, 469–474 (2006).
177. Sone, Y. et al. Nuclear translocation of phospholipase C-zeta, an egg-activating factor, during early embryonic development. *Biochem. Biophys. Res. Commun.* **330**, 690–694 (2005).
178. Fu, Y., Dominissini, D., Rechavi, G. & He, C. Gene expression regulation mediated through reversible m6A RNA methylation. *Nat. Rev. Genet.* **15**, 293 (2014).
179. Chen, Q. et al. Sperm tsRNAs contribute to intergenerational inheritance of an acquired metabolic disorder. *Science* **351**, 397–400 (2016).
180. Zini, A., Finelli, A., Phang, D. & Jarvi, K. Influence of semen processing technique on human sperm DNA integrity. *Urology* **56**, 1081–1084 (2000).
181. Xue, X. et al. Efficacy of swim-up versus density gradient centrifugation in improving sperm deformity rate and DNA fragmentation index in semen samples from teratozoospermic patients. *J. Assist. Reprod. Genet.* **31**, 1161–1166 (2014).
182. Henkel, R. R. & Schill, W. B. Sperm preparation for ART. *Reprod. Biol. Endocrinol.* **1**, 108 (2003).
183. Zaferani, M., Palermo, G. D. & Abbaspourrad, A. Strictures of a microchannel impose fierce competition to select for highly motile sperm. *Sci. Adv.* **5**, 2111 (2019).
184. Li, K. et al. Novel distance — progesterone — combined selection approach improves human sperm quality. *J. Transl. Med.* **16**, 1–10 (2018).
185. Tasoglu, S. et al. Exhaustion of racing sperm in nature-mimicking microfluidic channels during sorting. *Small* **9**, 3374–3384 (2013).
186. Nosrati, R., Graham, P. J., Liu, Q. & Sinton, D. Predominance of sperm motion in corners. *Sci. Rep.* **6**, 1–9 (2016).
187. Zaferani, M., Hon, S. & Abbaspourrad, A. Rheotaxis-based separation of sperm with progressive motility using a microfluidic corral system. *Proc. Natl Acad. Sci. USA* **115**, 8272–8277 (2018).
188. Kaupp, U. B., Kashikar, N. D. & Weyand, I. Mechanisms of sperm chemotaxis. *Annu. Rev. Physiol.* **70**, 93–117 (2008).
189. Huszar, G. et al. Hyaluronic acid binding by human sperm indicates cellular maturity, viability, and unreacted acrosomal status. *Fertil. Steril.* **79**, 1616–1624 (2003).
190. Simopoulou, M. et al. Improving ICSI: a review from the spermatozoon perspective. *Syst. Biol. Reprod. Med.* **62**, 359–371 (2016).

191. Liu, T. et al. Detection of apoptosis based on the interaction between annexin V and phosphatidylserine. *Anal. Chem.* **81**, 2410–2413 (2009).
192. Gil, M., Sar-Shalom, V., Sivira, Y. M., Carreras, R. & Checa, M. A. Sperm selection using magnetic activated cell sorting (MACS) in assisted reproduction: a systematic review and meta-analysis. *J. Assist. Reprod. Genet.* **30**, 479–485 (2013).
193. Galatioto, G. P. et al. May antioxidant therapy improve sperm parameters of men with persistent oligospermia after retrograde embolization for varicocele? *World J. Urol.* **26**, 97–102 (2008).
194. Jun, L. et al. Quantitative analysis of locomotive behavior of human sperm head and tail. *Biomed. Eng. IEEE Trans.* **60**, 390–396 (2013).
195. Zhang, Z. et al. An automated system for investigating sperm orientation in fluid flow. *IEEE Int. Conf. Robot. Autom*. https://doi.org/10.1109/ICRA.2016.7487551 (2016).
196. Hernandez-Herrera, P., Montoya, F., Rendón-Mancha, J. M., Darszon, A. & Corkidi, G. 3-D human sperm flagellum tracing in low SNR fluorescence images. *IEEE Trans. Med. Imaging* **37**, 2236–2247 (2018).
197. Saggiorato, G. et al. Human sperm steer with second harmonics of the flagellar beat. *Nat. Commun.* **8**, 1–9 (2017).
198. Friedrich, B. M., Riedel-Kruse, I. H., Howard, J. & Julicher, F. High-precision tracking of sperm swimming fine structure provides strong test of resistive force theory. *J. Exp. Biol.* **213**, 1226–1234 (2010).
199. Gade, H., Gaffney, E. A. & Smith, D. J. Nonlinear instability in flagellar dynamics: a novel modulation mechanism in sperm migration? *J. R. Soc. Interface* **7**, 1689–1697 (2010).
200. Zhang, Z. et al. Human sperm rheotaxis: a passive physical process. *Sci. Rep.* **6**, 23553 (2016).
201. Bukatin, A., Kukhtevich, I., Stoop, N., Dunkel, J. & Kantsler, V. Bimodal rheotactic behavior reflects flagellar beat asymmetry in human sperm cells. *Proc. Natl Acad. Sci. USA* **112**, 15904–15909 (2015).
202. Pérez-Cerezales, S. et al. Involvement of opsins in mammalian sperm thermotaxis. *Sci. Rep.* **5**, 16146 (2015).
203. Di Caprio, G. et al. 4D tracking of clinical seminal samples for quantitative characterization of motility parameters. *Biomed. Opt. Express* **5**, 690–700 (2014).
204. Di Caprio, G. et al. Holographic imaging of unlabelled sperm cells for semen analysis: a review. *J. Biophotonics* **8**, 779–789 (2015).
205. Suarez, S. S. & Pacey, A. A. Sperm transport in the female reproductive tract. *Hum. Reprod. Update* **12**, 23–37 (2006).
206. Gadêlha, H., Hernández-Herrera, P., Montoya, F., Darszon, A. & Corkidi, G. Human sperm uses asymmetric and anisotropic flagellar controls to regulate swimming symmetry and cell steering. *Sci. Adv.* **6**, eaba5168 (2020).
207. Elgeti, J., Kaupp, U. B. & Gompper, G. Hydrodynamics of sperm cells near surfaces. *Biophys J* **99**, 1018–1026 (2010).
208. Zhang, X. et al. Lensless imaging for simultaneous microfluidic sperm monitoring and sorting. *Lab. Chip* **11**, 2535 (2011).
209. Bazylewski, P. & Ezugwu, S. A review of three-dimensional scanning near-field optical microscopy (3D-SNOM) and its applications in nanoscale light management. *Appl. Sci.* **7**, 973 (2017).
210. Andolfi, L. et al. The application of scanning near field optical imaging to the study of human sperm morphology. *J. Nanobiotechnol.* **13**, 2 (2015).
211. Chemes, H. E. & Rawe, V. Y. Sperm pathology: a step beyond descriptive morphology. Origin, characterization and fertility potential of abnormal sperm phenotypes in infertile men. *Hum. Reprod. Update* **9**, 405–428 (2003).
212. Xu, J., Tehrani, K. F., Kner, P., States, U. & Avenue, C. Multicolor 3D super-resolution imaging by quantum dot stochastic optical reconstruction microscopy. *ACS Nano* **9**, 2917–2925 (2015).
213. Huang, B., Wang, W., Bates, M. & Zhuang, X. Three-dimensional super-resolution imaging by stochastic optical reconstruction microscopy. *Science* **319**, 810–814 (2008).
214. Chung, J. J. et al. CatSperζ regulates the structural continuity of sperm Ca^{2+} signaling domains and is required for normal fertility. *eLife* **6**, e23082 (2007).
215. Strünker, T. et al. The CatSper channel mediates progesterone-induced Ca 2+ influx in human sperm. *Nature* **471**, 382–386 (2011).
216. Gervasi, G., Xu, X., Carbajal-Gonzalez, B., Buffone, M. G. & Visconti, P. E. The actin cytoskeleton of the mouse sperm flagellum is organized in a helical structure. *J. Cell Sci.* **131**, 1–9 (2018).
217. Dunleavy, J. E., O'Bryan, M. K., Stanton, P. G. & O'Donnell, L. The cytoskeleton in spermatogenesis. *Reproduction* **157**, 53–72 (2019).
218. Paës, G., Habrant, A. & Terryn, C. Fluorescent nano-probes to image plant cell walls by super-resolution STED microscopy. *Plants* **7**, 1–9 (2018).
219. Aminski, C. L. F. K. Frontiers in structured illumination microscopy. *Optica* **3**, 667–677 (2016).
220. Gustafsson, M. G. Surpassing the lateral resolution limit by a factor of two using structured illumination microscopy. *J. Microsc.* **198**, 82–87 (2000).
221. Dan, D. et al. DMD-based LED-illumination super-resolution and optical sectioning microscopy. *Sci. Rep.* **3**, 1–7 (2013).
222. Chang, B. J., Chou, L. J., Chang, Y. C. & Chiang, S. Y. Isotropic image in structured illumination microscopy patterned with a spatial light modulator. *Opt. Express* **17**, 14710–14721 (2009).
223. Calvi, A. et al. SUN4 is essential for nuclear remodeling during mammalian spermiogenesis. *Dev. Biol.* **407**, 321–330 (2015).
224. Yeh, C. H. et al. SEPT12/SPAG4/LAMINB1 complexes are required for maintaining the integrity of the nuclear envelope in postmeiotic male germ cells. *PLoS ONE* **10**, e0120722 (2015).
225. Miller, M. R. et al. Unconventional endocannabinoid signaling governs sperm activation via the sex hormone progesterone. *Science* **352**, 555–9 (2016).
226. Baker, M. A., Hetherington, L., Ecroyd, H., Roman, S. D. & Aitken, R. J. Analysis of the mechanism by which calcium negatively regulates the tyrosine phosphorylation cascade associated with sperm capacitation. *J. Cell Sci.* **117**, 211–222 (2004).
227. Asquith, K. L., Baleato, R. M., McLaughlin, E. A., Nixon, B. & Aitken, R. J. Tyrosine phosphorylation activates surface chaperones facilitating sperm-zona recognition. *J. Cell Sci.* **117**, 3645–3657 (2004).
228. Awad, H., Khamis, M. M. & El-Aneed, A. Mass spectrometry, review of the basics: ionization. *Appl. Spectrosc. Rev.* **50**, 158–175 (2015).
229. Platt, M. D., Salicioni, A. M., Hunt, D. F. & Visconti, P. E. Use of differential isotopic labeling and mass spectrometry to analyze capacitation-associated changes in the phosphorylation status of mouse sperm proteins. *J. Proteome Res.* **8**, 1431–1440 (2009).
230. Ardito, F., Giuliani, M., Perrone, D., Troiano, G. & Lo Muzio, L. The crucial role of protein phosphorylation in cell signaling and its use as targeted therapy. *Int. J. Mol. Med.* **40**, 271–280 (2017).
231. Castillo, J. et al. Proteomic changes in human sperm during sequential in vitro capacitation and acrosome reaction. *Front. Cell Dev. Biol.* **7**, 295 (2019).
232. Drabovich, A. P. et al. Differential diagnosis of azoospermia with proteomic biomarkers ECM1 and TEX101 quantified in seminal plasma. *Sci. Transl. Med.* **5**, 212ra160 (2013).
233. Zerbinati, C. et al. Redox Biology Mass spectrometry pro fi ling of oxysterols in human sperm identi fi es 25- hydroxycholesterol as a marker of sperm function. *Redox Biol.* **11**, 111–117 (2017).
234. Hafiz, P. et al. Predicting implantation outcome of in vitro fertilization and intracytoplasmic sperm injection using data mining techniques. *Int. J. Fertil. Steril.* **11**, 184–190 (2017).
235. Comhaire, F., Messiaen, A. & Decleer, W. A mathematical model predicting the individual outcome of IVF through sperm-analysis: the role of the HaloSpermG2 DNA fragmentation test. *Med. Hypotheses* **117**, 50–53 (2018).
236. Farias-hesson, E. et al. Semi-automated library preparation for high-throughput DNA sequencing platforms. *J. Biomed. Biotechnol.* **2010**, 1–8 (2010).
237. Malm, J. et al. Semi-automated biobank sample processing with a 384 high density sample tube robot used in cancer and cardiovascular studies. *Clin. Transl. Med.* **4**, 27 (2015).
238. Litjens, G. et al. A survey on deep learning in medical image analysis. *Med. Image Anal. J.* **42**, 60–88 (2017).
239. Hicks, S. A. et al. Machine learning-based analysis of sperm videos and participant data for male fertility prediction. *Sci. Rep.* **9**, 1–10 (2019).
240. Sobieranski, A. C. et al. Portable lensless wide-field microscopy imaging platform based on digital inline holography and multi-frame pixel super-resolution. *Light. Sci. Appl.* **4**, 346 (2015).
241. Kanakasabapathy, M. K. et al. An automated smartphone-based diagnostic assay for point-of-care semen analysis. *Sci. Transl. Med.* **9**, 7863 (2017).
242. Carrilho, E., Martinez, A. W. & Whitesides, G. M. Understanding wax printing: a simple micropatterning process for paper-based microfluidics. *Anal. Chem.* **81**, 7091–7095 (2009).
243. Matsuura, K. et al. Paper-based diagnostic devices for evaluating the quality of human sperm. *Microfluid. Nanofluidics* **16**, 857–867 (2014).
244. Nosrati, R., Gong, M. M., Gabriel, C. S., Zini, A. & Sinton, D. Paper-based sperm DNA integrity analysis. *Anal. Methods* **8**, 6260–6264 (2016).
245. Ribas-Maynou, J. et al. Comprehensive analysis of sperm DNA fragmentation by five different assays: TUNEL assay, SCSA, SCD test and alkaline and neutral Comet assay. *Andrology* **1**, 715–722 (2013).
246. Eisenbach, M. & Giojalas, L. Sperm guidance in mammals — an unpaved road to the egg. *Nat. Rev. Mol. Cell Biol.* **7**, 276–285 (2006).
247. Vanderzwalmen, P. et al. Blastocyst development after sperm selection at high magnification is associated with size and number of nuclear vacuoles. *Reprod. Biomed. Online* **17**, 617–627 (2008).
248. Pandiyan, N. et al. in *Male Infertility A Clinical Approach* (Springer, 2016).
249. Rougier, N. et al. Changes in DNA fragmentation during sperm preparation for intracytoplasmic sperm injection over time. *Fertil. Steril.* **100**, 69–74 (2013).
250. Fink, M. & Taylor, M. A. in *A Clinician' s Guide to Diagnosis Sperm DNA and Chromatin Damage* (Springer, 2018).
251. Palermo, G. D., Colombero, L. T., Hariprashad, J. J., Schlegel, P. N. & Rosenwaks, Z. Chromosome analysis of epididymal and testicular sperm in azoospermic patients undergoing ICSI. *Hum. Reprod.* **17**, 570–575 (2002).
252. Lockwood, W. W., Chari, R., Chi, B. & Lam, W. L. Recent advances in array comparative genomic hybridization technologies and their applications in human genetics. *Eur. J. Hum. Genet.* **14**, 139–148 (2006).

Author contributions
Y.S., C.D., Z.Z. and K.J. contributed substantially to discussion of the content. C.D, Z.Z., G.S., L.-T.C. and Z.H. wrote the article. Y.S., S.M., C.L. and K.J. reviewed and/or edited the manuscript before submission.

Competing interests
The authors declare no competing interests.

Peer review information
Nature Reviews Urology thanks R. Dada, N. Garrido and R. Henkel for their contribution to the peer review of this work.